Astronomy & Astrophysics manuscript no. src October 24, 2007
(DOI: will be inserted by hand later)

INTEGRAL/IBIS all-sky survey in hard X-rays⋆

R. Krivonos[1,2], M. Revnivtsev[1,2], A. Lutovinov[2,1], S. Sazonov[1,2], E. Churazov[1,2], R. Sunyaev[1,2]

[1] Max-Planck-Institute für Astrophysik, Karl-Schwarzschild-Str. 1, D-85740 Garching bei München, Germany
[2] Space Research Institute, Russian Academy of Sciences, Profsoyuznaya 84/32, 117997 Moscow, Russia

the date of receipt and acceptance should be inserted later

Abstract.
We present results of an all-sky hard X-ray survey based on almost four years of observations with the IBIS telescope on board the INTEGRAL observatory. The dead time-corrected exposure of the survey is ~ 33 Ms. Approximately 12% and 80% of the sky have been covered to limiting fluxes lower than 1 and 5 mCrab, respectively. Our catalog of detected sources includes 400 objects, 339 of which exceed a 5σ detection threshold on the time-averaged map of the sky and the rest were detected in various subsamples of exposures. Among the identified sources, 213 are Galactic (87 low-mass X-ray binaries, 74 high-mass X-ray binaries, 21 cataclysmic variables, 6 coronally active stars, and other types) and 136 are extragalactic, including 131 active galactic nuclei (AGNs) and 3 clusters of galaxies. We obtained number–flux functions for AGNs and Galactic sources. The $\log N$–$\log S$ relation of AGNs (excluding blazars) is based on 69 sources with fluxes higher than $S_{\rm lim} = 1.1\times10^{-11}$ erg s^{-1} cm^{-2} (~ 0.8 mCrab) in the 17–60 keV energy band. The cumulative number–flux function of AGNs located at Galactic latitudes $|b| > 5^\circ$, where the survey is characterized by high identification completeness, can be described by a power law with a slope of 1.62 ± 0.15 and normalization of $(5.7 \pm 0.7) \times 10^{-3}$ sources per deg^2 at fluxes $> 1.43 \times 10^{-11}$ erg s^{-1} cm^{-2} (> 1 mCrab). AGNs with fluxes higher than $S_{\rm lim}$ make up $\sim 1\%$ of the cosmic X-ray background at 17–60 keV. We present evidence of strong inhomogeneity in the spatial distribution of nearby ($\lesssim 70$ Mpc) AGNs, which reflects the large-scale structure in the local Universe.

Key words. Surveys – X-rays: general – Galaxy: general – Galaxies: Seyfert – (Cosmology:) large-scale structure of Universe

1. Introduction

The INTEGRAL observatory (Winkler et al. 2003) has been successfully operating in orbit since its launch in 2002. Due to the high sensitivity and relatively good angular resolution of its instruments, in particular the coded-mask telescope IBIS (Ubertini et al. 2003), surveying the sky in hard X-rays is one of the primary goals of INTEGRAL. A number of papers have reported results of deep observations of relatively compact regions of the sky (e.g Revnivtsev et al. 2003a; Molkov et al. 2004; Krivonos et al. 2005a; Revnivtsev et al. 2006) and of systematic searches for sources over very large sky areas (e.g., Bird et al. 2006a,b). However, until recently it was difficult to use INTEGRAL data for source population studies, in particular extragalactic, because the coverage of the sky remained substantially incomplete. Therefore, in 2005–2006 we performed dedicated observations of the previously unobserved regions of the sky and thereby completed the most sensitive ever all-sky survey in hard X-rays. In this paper, we present a catalog of sources detected during the all-sky survey (Sect. 4), discuss the number–flux relations of Galactic and extragalactic hard X-ray sources (Sect. 5), and investigate the spatial distribution of local AGNs (Sect. 6).

2. Survey coverage and sensitivity

The present survey is based on observations performed during the first four years of the INTEGRAL mission. We used data from the ISGRI detector of the IBIS telescope, which is well suited for carrying out imaging surveys in hard X-rays. The coded-mask telescope IBIS provides a wide field of view of $28^\circ \times 28^\circ$ ($9^\circ \times 9^\circ$ fully coded) and moderate angular resolution of $12'$. The localization accuracy of <2–$3'$ is sufficiently good for searches of soft X-ray and optical counterparts and subsequent optical identification of newly discovered hard X-ray sources.

We used all public and proprietary data available to us. The observations were performed during spacecraft revolutions from 25 (end of December 2002) to 463

⋆ Based on observations with INTEGRAL, an ESA project with instruments and science data centre funded by ESA member states (especially the PI countries: Denmark, France, Germany, Italy, Switzerland, Spain), Czech Republic and Poland, and with the participation of Russia and the USA

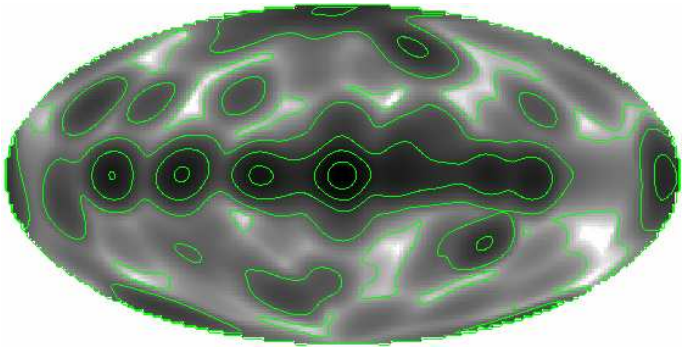

Fig. 1 Dead time-corrected exposure map of the survey. The green contours represent exposure levels of 10, 150, 800 ks, 2 and 4 Ms.

(June 2006). Importantly, our data set includes the special series of thirteen 200 ks-long extragalactic pointings (PI Churazov), which allowed us to complete the survey of the entire sky. Figure 2 shows the fraction of the sky covered by the survey as a function of the limiting flux for source detection with at least 5σ significance. Approximately 12% and 80% of the sky are covered down to 1 and 5 mCrab, respectively. After data cleaning and dead-time correction, the total exposure time of the survey is ~ 33 Ms.

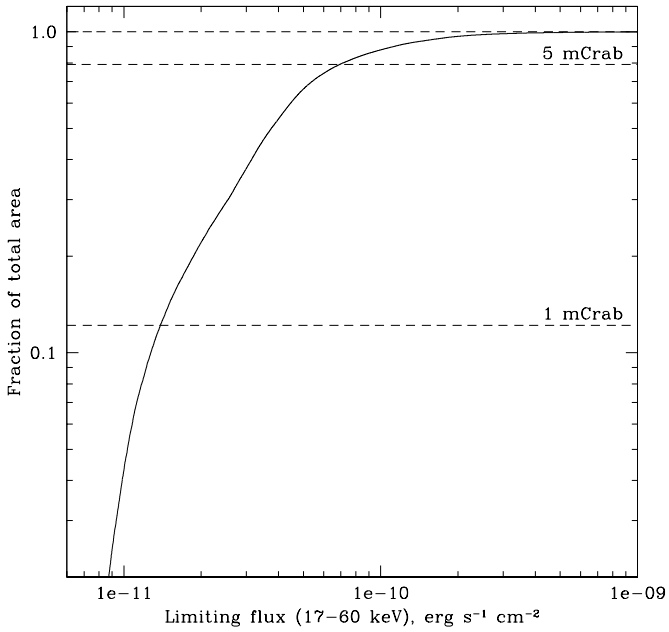

Fig. 2 Fraction of the sky surveyed as a function of the limiting flux for source detection with 5σ significance.

3. Data analysis

We analyzed the entire set of INTEGRAL observations at the level of individual pointings (science windows, SCWs), which have typical exposures of 2 ksec. For each observation, the IBIS/ISGRI raw events list was converted to a sky image in our working energy band (17–60 keV). The employed algorithm of image reconstruction was previously described by Revnivtsev et al. (2004a) and Krivonos et al. (2005a). Here we outline only those steps that are essential for the present study.

We first accumulated raw detector images in the 17–60 keV energy band and cleaned them from bad and noisy pixels. The reconstruction starts with rebinning the raw detector images onto a grid with a pixel size equal to 1/3 of the mask pixel size. This is close but not exactly equal to the detector pixel size. Therefore, the rebinning causes a moderate loss in spatial resolution but enables a straightforward application of standard coded-mask reconstruction algorithms (e.g., Fenimore et al. 1981, Skinner et al. 1981). Essentially, for each sky location, the flux is calculated as the total flux in those detector pixels that "see" that location through the mask minus the flux in those detector pixels that are blocked by the mask.

The image reconstruction is based on the DLD deconvolution procedure (see the notations in Fenimore et al. 1981), with a mask pixel corresponding to $n \times n$ detector pixels. The original detector is treated as $n \times n$ independent detectors, and $n \times n$ independent sky images are reconstructed and then combined into a single image. A point source in such an image is represented by a $n \times n$ square. In our case, this leads to the effective point spread function (PSF) being approximately a square of 3×3 detector pixels, or $12' \times 12'$. After summing a large number of individual images, the 2D shape of the PSF can be well approximated by a Gaussian with $\sigma = 1.25'$.

The periodic structures in the IBIS mask cause the appearance of parasitic peaks ("ghosts") in the images of real sources. We used an iterative procedure to eliminate such ghosts. For this purpose, we used a "current" catalog of sources, which was renewed each time a new bright source was detected. The image reconstruction was then redone for each observation containing the new source using the updated current catalog.

The case of a bright source

Since the pattern of the shadowgram cast by a point source through the mask is not ideally known, the ghost removal procedure is not perfect. Some photon counts can be left or oversubtracted at certain positions on the detector. This effect is usually small but can become significant for deep fields containing very bright sources. In this case, characteristic "crosses" and "rings" appear around the bright sources. The former artifact appears when the observational program of a bright source is dominated by starring pointings with a constant roll angle. A variable roll angle diminishes this effect but produces concentric structures. In practice this means that in regions with very bright sources, some source detections based on the criterion of exceeding a reasonable threshold, say 5σ, may be false. The level at which imperfect ghost removal starts to play a role depends on the observational pattern and typically corresponds to $\sim(3\text{–}5)\times10^{-3}$ of the flux of the

brightest source within the IBIS field of view. Therefore, the extracted list of excesses should always be checked "by eye" and cleaned out from such characteristic series of false detections around bright sources. It should be noted that such a cleaning introduces "dead zones" where a real source may be missed. We have verified that in the worst case, the total area of such zones does not exceed 100 deg^2, which constitutes a neglible fraction of the total area of our all-sky survey.

On applying the procedures described above, each observation is represented by a $28^\circ \times 28^\circ$ sky image with a pixel size of $4'$. The full analyzed data set contains 23,547 such images and comprises ~ 35 Ms (dead time-corrected) worth of observations. We applied an additional filtering to the resulting images using information about the residual (after subtraction of point sources) *rms* signal-to-noise variations in the images. Those images having $rms > 1.05$ were excluded from the analysis. This resulted in an additional rejection of $\sim 7\%$ of the pointings and finally left us with ~ 33 Ms worth of clean observations.

An analysis of mosaic images built from observations covering the whole sky is complicated by various effects of projections onto a 2D plane. The most significant one is distortions of the point spread function (PSF) at positions far from the center of the projection. This leads to uncertainties in estimating the source position and flux. To avoid this effect, we followed an approach that had been developed for analyzing data distributed on a sphere. Specifically, we used a number of subroutines from the HEALPIX package (**H**ierarchical **E**qual **A**rea iso**L**atitude **Pix**elization of a sphere, Górski et al. 2005) to build a mosaiced sky. This technique provides an equal-area pixelization of the sphere and allows us to analyze all of the data uniformly. We produced a HEALPIX-based map of the whole sky with 12M pixels, which corresponds to a $\sim 3.4'$ size of each sky pixel. The map was constructed by projecting individual IBIS/ISGRI images onto the HEALPIX all-sky frame.

3.1. Detection of sources

We searched for sources on three time scales – in individual SCWs ($\sim$2 ks exposure time, typical sensitivity 20–30 mCrab), on images integrated over individual satellite orbits ($\sim$200 ks, $\sim$ 4 mCrab), and on the time-averaged all-sky map ($\sim$33 Ms).

The detection of sources was performed using $20^\circ \times 20^\circ$ projections of the HEALPIX all-sky image. Since adjacent pixels in these images (pixel size $\sim 4'$) are smaller that the instrumental PSF, we convolved the images with a Gaussian filter that mimics the effective instrumental PSF ($\sigma = 1.25'$).

The signal-to-noise ratio distribution of pixels is dominated by the statistical noise and can be described by a Gaussian. In those sky regions that contain very bright point sources, the *rms* scatter of signal-to-noise ratios increases. However, this mainly occurs due to the presence of unsubtracted ghosts, which can be found by eye and removed.

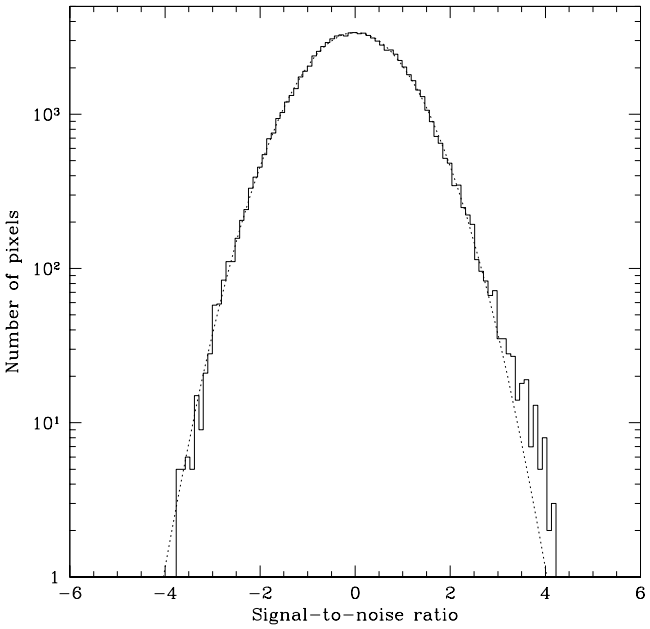

Fig. 3 Signal-to-noise ratio distribution (solid histogram) of the number of pixels in a $20^\circ \times 20^\circ$ projection image of the sky around the position $15h\ 28m\ 00.0s$, $-28^\circ\ 00m\ 00s$ (J2000). The dotted line represents the normal distribution with unit variance and zero mean.

There are small misalignments between the mask grid and the detector pixels, which cause imperfect redistribution of counts over the mask-aligned detector grid. However, this effect is minor, because the correlation length of the noise in the projected images is smaller than the size of the applied Gaussian filter. As a result, the originally measured variance of the distribution of pixel significances is slightly less than unity. To correct for this, we implemented a uniform rescaling of the error map for each sky projection. The correction factor was determined from each HEALPIX projection image and found to vary between 0.9 and 1.0. For sky fields containing a large number of point sources or for images of poor quality, the mentioned effect becomes less important than systematic biases introduced by the image reconstruction algorithm (Sect. 3). In such cases, the correction factor cannot be properly estimated, and so we adopted it to be not greater than unity. In Fig. 3 we show the signal-to-noise ratio distribution of the pixels of a $20^\circ \times 20^\circ$ corrected sky map centered on some arbitrary position. This distribution (except for the positive bright tail produced by real sources) can be described by the normal distribution with unit variance and zero mean.

We next specified a detection threshold in units of this clean "sigma" to search for sources in images. The lists of source candidates were then cleaned by eye from excesses forming characteristic patterns around bright sources.

Taking into account the IBIS/ISGRI angular resolution, the all-sky map and maps accumulated during single revolutions contain $\sim 10^6$ and 3×10^7 statistically independent pixels, respectively. We adopted the corresponding detection thresholds of $(S/N)_{\rm lim} > 5\sigma$ and $(S/N)_{\rm lim} > 5.5\sigma$ to ensure that the final catalog contains less than 1–2 spurious sources.

Apart from the main search described above, we detected several sources in special extended series of observations such as the deep surveys of the Sagittarius and Crux spiral arm tangent regions (Molkov et al. 2004; Revnivtsev et al. 2006). Some of these sources fall below our detection threshold (5σ) on the all time-averaged map, which probably indicates their strong variability or transient nature.

We emphasize that for statistical studies only those sources from the catalog that have time-averaged statistical significance higher than 5σ (see the flux column in Table 1 below) should be used.

3.2. Localization accuracy

We determined the positions of sources by fitting the centroid of a 2D gaussian ($\sigma = 1.25'$) to the peak of the PSF-convolved source image. To estimate the accuracy of this method, we built the distribution of deviations of the measured positions of sources with known cataloged locations for a large number of INTEGRAL observations. The positional accuracy of sources detected by IBIS/ISGRI depends on the source significance (Gros et al. 2003; Bird et al. 2006a). The estimated 68% confidence intervals for sources detected at 5–6, 10, and $> 20\sigma$ are $2.1'$, $1.5'$, and $< 0.8'$, respectively.

4. Catalog

We detected a total of 400 sources in the 17–60 keV energy band over the whole sky. The full list of sources is presented in Table 1, and its content is described below.

Column (1) – source number in the catalog.

Column (2) – source name. For sources whose nature was known before their detection by INTEGRAL, their common names are given. Sources discovered by INTEGRAL or those whose nature was established thanks to INTEGRAL are named "IGR"

Columns (3,4) – source Equatorial (J2000) coordinates.

Column (5) – time-averaged source flux in mCrab units. A flux of 1 mCrab corresponds to 1.43×10^{-11} erg s^{-1} cm^{-2} for a source with a Crab-like spectrum.

Column (6) – general astrophysical type of the object: LMXB (HMXB) – low- (high-) mass X-ray binary, AGN – active galactic nucleus, SNR/PWN – supernova remnant, CV – cataclysmic variable, PSR – isolated pulsar or pulsar wind nebula, SGR – soft gamma repeater, RS CVn – coronally active binary star, SymbStar – symbiotic star, Cluster – cluster of galaxies.

Column (7) – additional notes and/or alternative source names.

Column (8) – references. These are mainly provided for new sources and are related to their discovery and/or nature.

We note that Bird et al. (2006b) have recently performed a similar hard X-ray survey using INTEGRAL/IBIS/ISGRI data. The catalog of these authors contains 421 sources detected in five energy bands spanning 18–100 keV. Although a detailed comparison of this catalog with ours goes beyond the scope of the present paper, we may mention some important differences: (i) our dataset covers a number of extragalactic regions not covered by the survey of Bird et al. (2006b), on the other hand their dataset contains a considerable amount of data not available to us; (ii) Bird et al. (2006b) used the standard INTEGRAL OSA software, whereas we used a software developed at the Space Research Institute (Moscow, Russia); (iii) the detection criterion adopted in our work allows not more than 1–2 spurious sources to be present in the whole catalog, while the catalog of Bird et al. (2006b) may, by construction, contain considerably more spurious sources.

4.1. Some peculiar sources

Galactic Center source IGR J17456−2901

The sky density of hard X-ray sources is not very high – in general $N(> 1\text{mCrab}) < 0.1$ deg^{-2}, therefore the angular resolution of the IBIS telescope ($\sim 12'$) is usually sufficient to prevent source confusion. The only exceptional region is the Galactic center: in the close vicinity (within 1°) of Sgr A*, IBIS sees 10 sources.

At the position of Sgr A* there is an additional hard X-ray excess, IGR J17456−2901. This source was originally reported by Revnivtsev et al. (2004c) and erroneously associated with the X-ray burster AX J17456−2901. Subsequent studies of this source demonstrated that it is extended (Neronov et al. 2005; Bélanger et al. 2006) and is probably the superposition of a large number of faint point sources located in the Galactic nuclear stellar cluster (Krivonos et al. 2005b). Note that, as is shown by Bélanger et al. (2006), at higher energies ($\sim$ 70–100 keV), the position of the centroid of the excess is displaced with respect to Sgr A*, indicating that the nature of the high-energy source may be different from that of the 17–60 keV emission.

RX J1713.7−3946

Since IBIS is a coded-mask telescope, it is not well suited for studying sources more extended than its angular resolution. However, if a source is only somewhat larger than the instrumental PSF, it is possible to obtain some limited information about the spatial structure of the source (see e.g. Renaud et al. 2006a,b).

In particular, in our catalog there are four extended sources that are not much larger than the IBIS PSF ($\sim$

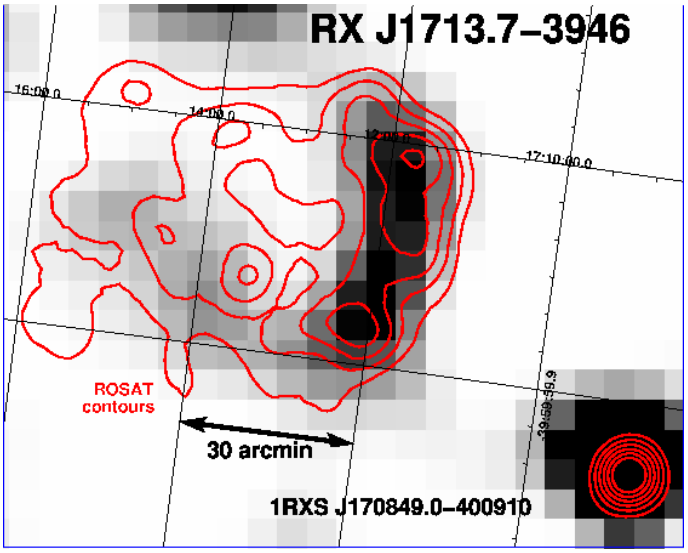

Fig. 4 INTEGRAL/IBIS hard X-ray (17–60 keV) image of the supernova remnant RX J1713.7−3946. The gray scale on the map is proportional to hard X-ray flux. The map obtained by ROSAT in the soft X-ray (0.5–2.5 keV) band is shown by contours.

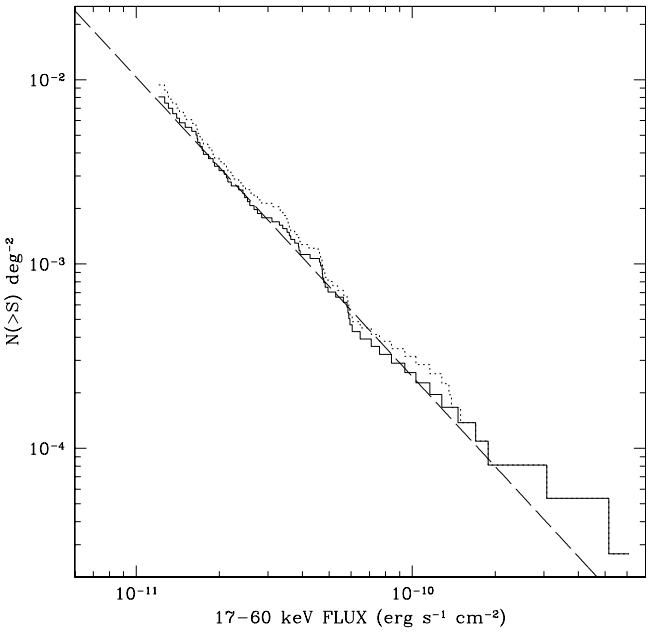

Fig. 5 Cumulative $\log N$–$\log S$ distribution of non-blazar AGNs in the energy band 17–60 keV obtained in the extragalactic sky ($|b| > 5°$, solid histogram). The best-fitting power law with a slope of 1.62 ± 0.15 and normalization of $(5.7 \pm 0.7) \times 10^{-3}$ deg^{-2} at a flux of 1 mCrab is shown by the dashed line. The dotted curve represents the $\log N$–$\log S$ distribution of all extragalactic sources including blazars and clusters of galaxies (except for unidentified sources).

12′): three clusters of galaxies (Oph, Perseus, and Coma) and the supernova remnant RX J1713.7−3946.

It is clearly seen (Fig. 4) that the supernova remnant RX J1713.7−3946 exhibits clear extended structure (visible size in hard X-rays $\sim 24'$). The significance of the hard X-ray detection varies along the extended structure between 4σ and 5σ (the statistical significance of the total extended emission is $> 10\sigma$). The total exposure for this region is 5.3 Ms (dead time-corrected). To test the stability of the apparent spatial feature, we split the entire period of observations into four intervals and examined them individually. The extended structure is clearly present in each image and looks stable against the background of variable noise.

The supernova remnant RX J1713.7−3946 was discovered in soft X-rays during the ROSAT all-sky survey (Pfeffermann & Aschenbach 1996). An extended elliptical structure was found with a maximum extent of 70′ (see the red contours in Fig. 4). The non-detection of emission lines in the X-ray spectrum of RX J1713.7−3946 (ASCA, Koyama et al. 1997; Slane et al. 1999) was regarded as an indication that the observed X-rays is non-thermal emission from an expanding shell.

Recently, very high-energy (VHE) gamma-ray emission was discovered from the remnant by the H.E.S.S. experiment (Aharonian et al. 2006). The spatial correlation of the VHE emission intensity with the X-ray morphology confirms that cosmic-ray particles are being accelerated in the shell.

Here we report a detection of RX J1713.7−3946 in hard X-rays. The hard X-ray emission is probably synchrotron emission of 100-TeV electrons accelerated in the shell (Koyama et al. 1995).

5. Extragalactic sources – AGNs

All sources in our catalog can be separated into two main classes – galactic and extragalactic (mainly AGNs). Under the assumption that AGNs are uniformly distributed over the sky (which is only a crude approximation of the real situation, see Sect. 6), we can construct the deepest ever number-flux function of hard X-ray emitting AGNs.

The catalog contains 131 objects[1] identified as AGNs (see also Sazonov et al. 2007 [2]). Of these, 94 have statistical significance higher than 5σ on the time-averaged map, including 86 emission-line AGNs (non-blazars) and 8 blazars. There are also 40 unidentified sources detected on the average map. The relative fraction of unidentified sources is much smaller for the extragalactic sky ($|b| > 5°$) than for the whole sky: the corresponding numbers of non-blazar AGNs and unidentified sources are 69 and 6.

[1] Three additional sources: IGR J02466−4222, IGR J02524−0829, and IGR J18578−3405 have a suspected AGN origin.

[2] After publication of the INTEGRAL AGN catalog by Sazonov et al. (2007), four sources have been added to the AGN list: IGR J18249−3243 (Bassani et al. 2006), ESO 005-G004, IGR J14561−3738, and SWIFT 0920.8−0805

Since INTEGRAL observations cover the sky inhomogeneously, in constructing number-flux functions we should take the sensitivity map into account. In Fig. 5 we show the cumulative $\log N$–$\log S$ distribution of non-blazar AGNs derived at $|b| > 5^\circ$ (excluding the 7 unidentified sources). It can be well fit by a power law: $N(> S) = AS^{-\alpha}$. Using a maximum-likelihood estimator (see e.g. Crawford et al. 1970), we determined the best-fit values of the slope and normalization: $\alpha = 1.62 \pm 0.15$ and $A = (5.7 \pm 0.7) \times 10^{-3}$ deg^{-2} at $S = 1$ mCrab. This implies that AGNs with fluxes exceeding our effective threshold $S_{\rm lim} = 0.8$ mCrab account for $\sim 1\%$ of the intensity of the cosmic X-ray background in the 17–60 keV band, which was recently re-measured by INTEGRAL (Churazov et al. 2007).

We previously (Krivonos et al. 2005a) constructed a number–flux relation of extragalactic sources in a relatively small region of the sky ($45^\circ \times 45^\circ$) around the Coma cluster of galaxies. The deep ($\sim$ 500 ks) observations of the Coma were used to study a sample of 12 serendepitously detected sources in that field. After correcting for the expected number of false detections and fitting the resulting $\log N$–$\log S$ relation by a power law with the Euclidean-geometry slope of 3/2, the surface density of hard X-ray sources above a 20–50 keV flux threshold of 10^{-11} erg s^{-1} cm^{-2} ($\sim$ 1 mCrab) was found to be $(1.4 \pm 0.5) \times 10^{-2}$ deg^{-2}. This value is significantly higher than the average surface number density of AGNs in the $|b| > 5^\circ$ sky, determined above, which probably reflects the large-scale overdensity of galaxies in the general direction of the Coma cluster (see Sect. 6).

Using the derived $\log N$–$\log S$ distribution, we can compare the numbers of AGNs detected during the survey in different parts of the sky with the numbers expected under the assumption of uniform spatial distribution of sources. We find good agreement between these numbers within the statistical errors for $15^\circ \times 360^\circ$ strips cut parallel to the Galactic plane (Fig. 6). Even in the Galactic plane region ($|b| < 5^\circ$), which was excluded from our calculation of the number-flux function, the expected number of AGNs exceeding the detection threshold (18.4) is compatible with the number of detected and identified AGNs (16). This suggests that most of the unidentified sources in the Galactic plane region are of Galactic, rather than extragalactic origin. This tentative conclusion of course rests on our assumption that AGNs are distributed uniformly on very large scales over the sky, which is in fact approximately true only for relatively distant objects ($D \gtrsim 70$ Mpc, see the next Section) and much less so for more nearby AGNs, which constitute approximately half of our sample.

If we now include all the identified AGNs detected in the Galactic plane region into the calculation of the AGN number–flux function (thus increasing the total number of non-blazar AGNs to 86 and extending the calculation to the whole sky), we find $\alpha = 1.50 \pm 0.13$ and $A = (5.4 \pm 0.6) \times 10^{-3}$ deg^{-2} at 1 mCrab, i.e. virtually the same values as for the $|b| > 5^\circ$ sky.

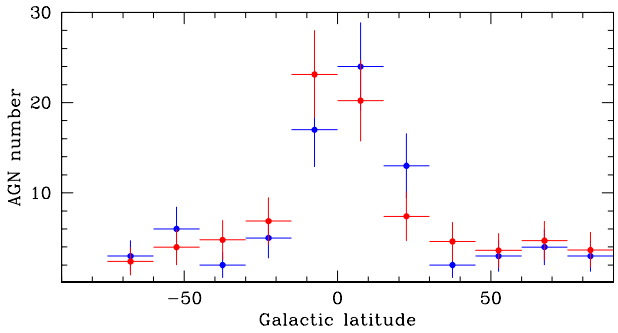

Fig. 6 Expected numbers of AGNs (red) in 15°-wide Galactic-latitude strips (integrated over all Galactic longitudes) and the corresponding numbers of actually detected and identified AGNs (blue). The involved statistical uncertainties are shown by error bars.

6. Signatures of large-scale structure in the population of hard X-ray AGNs

It is now widely accepted that practically every galaxy in the local Universe has a supermassive black hole and some of these black holes are AGNs with widely ranging luminosities (see e.g., Richstone et al. 1998; Kormendy 2001, for a review). Therefore, it is reasonable to assume that the space density of X-ray emitting AGNs is proportional to that of normal galaxies.

The spatial distribution of galaxies in the local Universe is inhomogeneous. The gravitational attraction of matter in the Universe has formed different structures with sizes[3] up to $\sim$ 100 Mpc. On larger scales, matter is distributed more or less uniformly, whereas on smaller scales there is strong inhomogeneity. The contrast in matter density between galaxy concentrations and voids can reach an order of magnitude and more (see e.g. Rees 1980; Davis & Peebles 1983; Bahcall & Burgett 1986). As our sample of hard X-ray emitting AGNs mostly probes the nearby Universe out to distances $\sim$ 200 Mpc, we have the possibility to see similarly strong inhomogeneities in the distribution of nearby AGNs.

To this end, we estimated the space densities of AGNs in different directions of the sky. Due to the relatively small size of our sample, we assumed that the AGN number density is constant along a given line of sight while the shape of the AGN luminosity function is invariant in the local Universe. We adopted this shape from Sazonov et al. (2007), who calculated the all-sky average hard X-ray luminosity function using the same sample of AGNs as in the present study.

Under these assumptions and using the sensitivity map of the survey, we determined the normalization of the luminosity function within spherical cones drawn around multiple directions in the sky through comparison of the expected and measured numbers of AGNs in these cones.

[3] Hereafter we adopt $H_0 = 73$ km s^{-1} Mpc^{-1}.

We adopted the half-opening angle of the cones to be $\theta = 45^\circ$ in order to achieve reasonably good angular resolution of the resulting map and still have a significant number of AGNs in each cone. To optimize our sensitivity to anisotropies in the spatial distribution of AGNs, we restricted ourselves to distances < 70 Mpc, at which maximal contrasts in galaxy numbers are expected (see e.g. Rowan-Robinson et al. 2000).

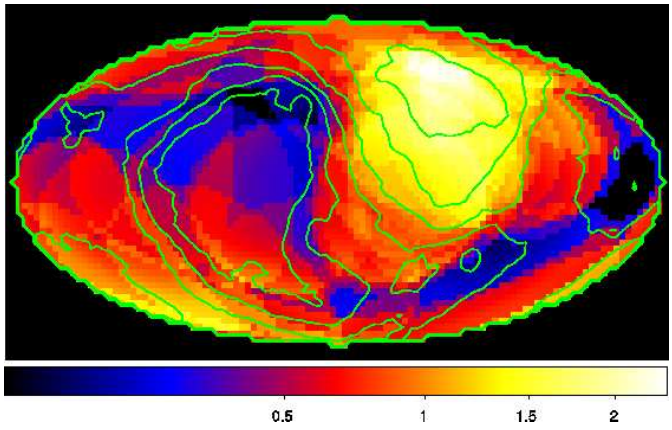

Fig. 7 2D-map of the AGN number density in the local Universe. This map was constructed in Galactic coordinates using the sample of 39 AGNs located at distances $D < 70$ Mpc. Shown for each pixel is the estimated normalization of the AGN luminosity function within a spherical cone with a half-opening angle of 45° around that direction. The density is given in units of 2×10^{-4} Mpc^{-3} at luminosities higher than 10^{42} erg s^{-1} (17–60 keV), which is the average local density of AGNs (Sazonov et al. 2007). Green contours show the surface number density of galaxies detected during the IRAS PSCz survey at distances $D < 70$ Mpc.

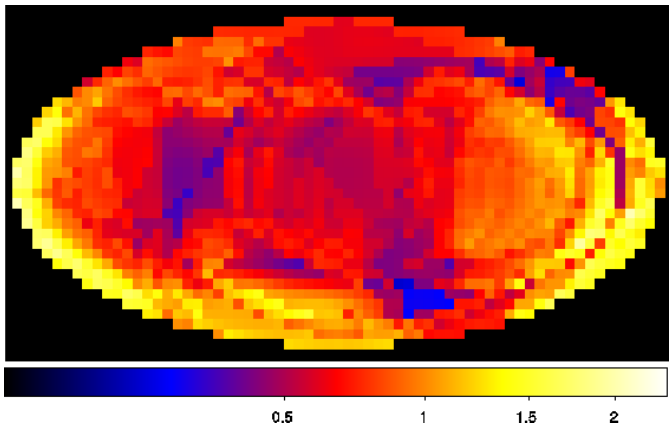

Fig. 8 2D-map of the number density of AGNs at distances $D > 70$ Mpc. See Fig. 7 for the description. This map is based on 40 obejcts.

In Sect. 3 we demonstrated that most of the extragalactic objects detectable by INTEGRAL in the Galactic plane region are probably already identified, hence we can use for our analysis the all-sky sample of AGNs.

The resulting map of the number density of nearby AGNs over the sky is shown in Fig. 7. The density is given in units of 2×10^{-4} Mpc^{-3} at luminosities higher than 10^{42} erg s^{-1} (17–60 keV), which is approximately the average local density of AGNs (Sazonov et al. 2007). Prominent large-scale concentrations of AGNs can be seen in the northern (to the right) and southern (to the left) Galactic hemispheres. We can assess the statistical significance of these anisotropies by considering the density measurements in statistically independent regions of the sky. Given the relatively large opening angle of our sampling cone, there are only 12 such independent directions on the whole sky. Since in our case the estimated density values are strongly affected by Poisson statistics, we constructed a maximum likelihood estimator in the form $L = \sum \log P_x(n)$, where $P_x(n)$ is the probability to detect n sources in our detection cone if the expected number of sources is x. The probability that the measured AGN number density distribution is a statistical realization of a homogeneous distribution is 8.7×10^{-4}.

If we take into account that the high and low AGN number density regions well correlate with known (from surveys of infrared galaxies, e.g. Rowan-Robinson et al. 2000, and X-ray clusters of galaxies, e.g. Kocevski & Ebeling 2006) over- and under-dense regions in the local Universe, respectively, the statistical significance of the found spatial inhomogeneity will be much higher.

The discovered anisotropy of AGNs agrees well with the known distribution of matter in the local Universe. The large-scale feature in the northern Galactic hemisphere is consistent with the position of the highest mass concentrations in the local Universe: the nearby Virgo cluster (~ 18 Mpc, $\sim 1.2 \times 10^{15} M_\odot$ Fouqué et al. 2001; Tonry et al. 2000) and the more distant and massive Great Attractor (~ 65 Mpc, $(1\text{–}5) \times 10^{16} M_\odot$, Lynden-Bell et al. 1988; Tonry et al. 2000). The southern structure is consistent with the Perseus-Pisces supercluster (~ 50 Mpc, $(7\text{–}9) \times 10^{15} M_\odot$, Hanski et al. 2001).

To better demonstrate the similarity between the distributions of hard X-ray emitting AGNs and matter over the sky, we used the IRAS PSC redshift survey (Saunders et al. 2000). We selected galaxies located at distances < 70 Mpc and have far-infrared flux $S_{60\mu m} > 1$ Jy. The IRAS PSCz survey covers approximately 83% of the sky due to presence of so-called Zone of avoidance, sky region to the north and to the south from the Galactic equator where Galaxy obcures the IR emission. In order to fill this gap during the construction of the map of densities of IR galaxies we assumed that the number density of galaxies hidden behind the Galactic plane (10 degrees to the north and to the south of the equator) is constant and equals to the all-sky average value. Contours of the number density map of IRAS galaxies are shown in Fig. 7.

We emphasize that this comparison is rather approximate and only reflects the distribution of the projected mass. A detailed study of the correlation between the spatial distributions of hard X-ray emitting AGNs and matter in the local Universe will be presented elsewhere.

It is obvious from the above discussion that any estimate of the AGN surface number density based on a small area of the sky may be significantly biased. This was apparently the case for our survey in the $\sim 45^\circ \times 45^\circ$ region around the Coma cluster (Krivonos et al. 2005a), where a high surface number density of relatively nearby ($D \lesssim 70$ Mpc) AGNs was found (see Sect. 5). Indeed, the observed region is located approximately in the direction of the prominent large-scale structure in the northern Galactic hemisphere (see Fig. 7). To better demonstrate the strong contrast in the distribution of AGNs over the sky, we calculated the sensitivity-corrected $\log N$–$\log S$ distributions of AGNs in the two hemispheres defined by the direction of motion of the Local Group: $l = 268^\circ, b = 27^\circ$, as measured by IRAS (Lahav et al. 1988). These distributions are shown in Fig. 9. The counts of bright sources ($S \gtrsim 10^{-10}$ erg s^{-1} cm^{-2}), for which our survey is almost 100% complete in both hemispheres, exhibit a contrast as high as 11 : 1.

In addition, we explicitly calculated the AGN luminosity functions in both hemispheres defined above and found their shapes to be consistent with that of the all-sky average luminosity function determined by Sazonov et al. (2007). This confirms that the found anisotropy mostly reflects the inhomogeneous distribution of matter in the local Universe rather than generic variations of the AGN luminosity function.

Figure 9 demonstrates that most of the observed anisotropy in the distribution of AGNs over the sky is due to closest (brightest) AGNs. Inclusion of sources located at progressively larger distances is expected to decrease the surface number density variations over the sky (Rowan-Robinson et al. 2000). To demonstrate this, we built a map of the number density of AGNs located at $D > 70$ Mpc (Fig. 8), which should be compared with that for nearby AGNs ($D < 70$ Mpc, Fig. 7). It can be seen that the more distant AGNs are distributed more uniformly across the sky, although their distribution is still only marginally consistent with a homogeneous one: the corresponding probablity is 10^{-2}.

The open circles in Fig. 9 show the $\log N$–$\log S$ distribution previously obtained in the Coma region. This number-flux relation lies higher than the all-sky average due to the overdensity of galaxies in this relatively small region of the sky (1,243 sq. deg), including two bright AGNs, NGC 4151 and NGC 4388. As a result, the resolved fraction of the CXB in this region is also high, $\sim 3\%$. As was already mentioned above, the resolved fraction of the CXB for the whole sky is only $\sim 1\%$. This last value is consistent with that reported by Beckmann et al. (2006) based on their analysis of INTEGRAL observations covering 25,000 sq. deg of the sky.

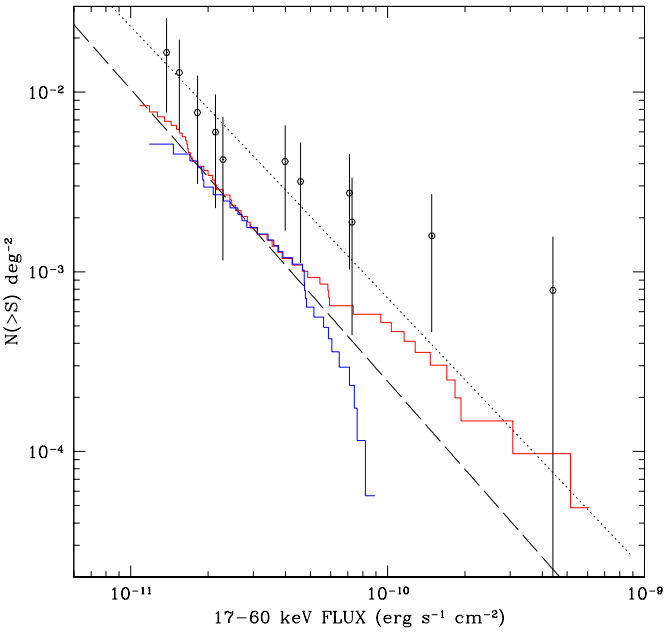

Fig. 9 Number-flux functions of extragalactic sources (excluding blasars and clusters of galaxies) measured in different sky regions. The $\log N$–$\log S$ relations for sources in two hemispheres, in the direction of the IRAS dipole $l = 268^\circ$, $b = 27^\circ$ (Lahav et al. 1988) and in the opposite direction, are shown by the red and blue histogram, respectively. The dashed line represents the best-fitting $\log N$–$\log S$ distribution for the entire sky excluding the Galactic plane ($|b| > 5^\circ$, see Fig. 5). The open circles with error bars represent the number-flux relation of extragalactic sources obtained in the $45^\circ \times 45^\circ$ region around the Coma cluster (Krivonos et al. 2005a) in the 20–50 keV energy band. The flux was converted to the 17–60 keV energy band assuming Crab spectrum. The dotted line shows the corresponding $N \propto S^{-3/2}$ fit.

7. Galactic sources

The presence of a large number of Galactic sources in the INTEGRAL all-sky catalog is obvious from the large overdensity of sources near the Galactic plane. For demonstration we built sensitivity-corrected cumulative number-flux functions for all ($> 5\sigma$) sources in 15° Galactic-latitude bins. The derived surface number density of sources as a function of Galactic latitude is shown in Fig. 10.

The vast majority of sources in the Galactic plane are low- and high-mass X-ray binaries ($> 70\%$ in total, excluding unidentified sources). The number-flux function of all sources at $|b| < 5^\circ$ (Fig. 11), is much flatter than that of extragalactic sources at $|b| > 5^\circ$ (Forman et al. 1978) and reflects the luminosity functions of the dominant Galactic source populations (see e.g. Grimm et al. 2002). A detailed study of Galactic sources based on the INTEGRAL all-sky survey will be presented elsewhere.

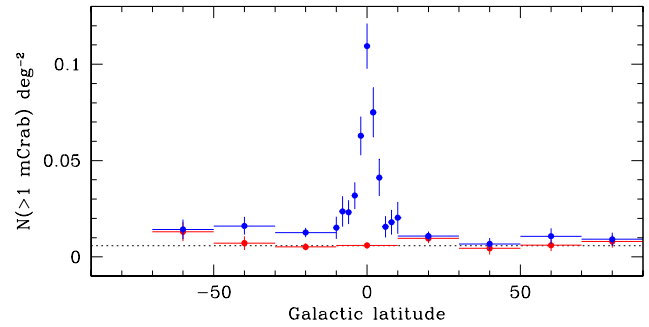

Fig. 10 Surface number density of ($> 5\sigma$) sources with flux > 1 mCrab as a function of Galactic latitude. Blue and red points represent all and (identified) extragalactic sources, respectively. The dashed line represents the normalization of the all-sky extragalactic $\log N$–$\log S$ function.

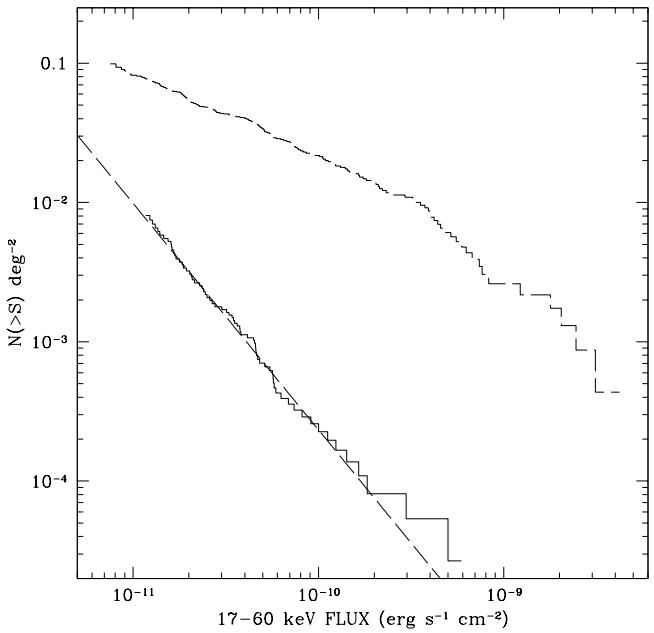

Fig. 11 Cumulative $\log N$–$\log S$ distribution in the energy band 17–60 keV of all sources in the Galactic plane region ($|b| < 5°$, dashed histogram) in comparison with that of AGNs at high latitudes ($|b| > 5°$, solid histogram). The dashed line represents the best-fitting power law to the number-flux relation of AGNs.

8. Conclusion

We have presented the all-sky hard X-ray (17–60 keV) survey performed by the IBIS coded-mask telescope of the INTEGRAL observatory. The total dead-time corrected exposure of the survey is 33 Ms. 12% and 80% of the whole sky have been covered down to limiting fluxes of 1 and 5 mCrab, respectively. The survey allowed us for the first time to study the population of hard X-ray sources in an unbiased manner, without strong influence of limited sky coverage.

Our catalog contains 400 detected sources. Of these, 213 are of Galactic origin (87 LMXBs, 74 HMXBs, 21 CVs, 6 active stars, and other types) and 136 are extragalactic, including 131 AGNs, 3 AGN candidates, and 3 clusters of galaxies. There remain 48 (including 40 detected with more than 5σ significance on the time-averaged map) unidentified sources, only 6 of which are located in the extragalactic sky ($|b| > 5°$). The catalog includes 137 sources discovered by INTEGRAL, 15 of which are reported here for the first time.

A number of sources detected by INTEGRAL/IBIS have counterparts in the TeV energy band. In this paper we for the first time presented the map of extended hard X-ray (17–60 keV) emission of the supernova remnant RX J1713.7−3946.

We explored the spatial distribution of AGNs in the local Universe. The cumulative $\log N$–$\log S$ function of AGNs derived away from the Galactic plane (at $|b| > 5°$) can be well fit by a power law $N(> S) = (5.7 \pm 0.7) \times 10^{-3} S^{-1.62 \pm 0.15}$ deg^{-2} (fluxes in mCrab units). This implies that $\sim 1\%$ of the CXB at 17–60 keV is directly resolved by INTEGRAL.

We demonstrated that local ($\lesssim 70$ Mpc) AGNs are inhomogeneously distributed in space, largely following the large-scale structure. In particular, significant concentrations of AGNs were found in the regions of the sky around the Virgo cluster, the Great Attractor, and the Perseus-Picses supercluster.

Acknowledgements. The INTEGRAL data used here were obtained from the European and Russian INTEGRAL Science Data Centers. The work was supported by the President of the Russian Federation (through the program of support of leading scientific schools, project NSH-1100.2006.2), by the Presidium of the Russian Academy of Sciences/RAS (the program "Origin and evolution of stars and galaxies"), by the Division of Physical Sciences of the RAS (the program "Extended objects in the Universe"), and by the Russian Basic Research Foundation (projects 05-02-16540 and 04-02-17276). AL acknowledges the support from the Russian Science Support Foundation.

9. References for the catalog

(1) Donato et al. (2005), (2) Sazonov et al. (2005), (3) Masetti et al. (2004), (4) Masetti et al. (2006c), (5) Brandt et al. (2005), (6) Sunyaev et al. (2003a), (7) Masetti et al. (2006e), (8) Masetti et al. (2006b), (9) Bassani et al. (2006), (10) Sguera et al. (2006), (11) Lutovinov et al. (2004a), (12) Lubinski et al. (2005), (13) den Hartog et al. (2004a), (14) Grebenev et al. (2004b), (15) Smith et al. (2006), (16) Kretschmar et al. (2004), (17) Chernyakova et al. (2005a), (18) in't Zand & Heise (2004), (19) Rodriguez et al. (2004), (20) Morelli et al. (2006), (21) Revnivtsev et al. (2004b), (22) Kuulkers et al. (2006), (23) Revnivtsev et al. (2006), (24) Lutovinov & Revnivtsev (2003), (25) Lutovinov et al. (2005a), (26) Bykov et al.

(2004), (27) Bassani et al. (2005), (29) Pavlinskii et al. (1992), (30) Lutovinov et al. (2003c), (31) in't Zand (2005), (32) Bikmaev et al. (2006a), (33) Negueruela & Smith (2006), (34) Produit et al. (2003), (35) Barlow et al. (2005), (36) Barlow et al. (2006), (37) Walter et al. (2006), (38) Molkov et al. (2004), (39) Bykov et al. (2006), (40) Liu et al. (2000), (41) Liu et al. (2001), (42) Rodriguez et al. (2005), (43) den Hartog et al. (2005), (44) Bird et al. (2006a), (45) den Hartog et al. (2004b), (46) Ubertini et al. (2005), (47) Malizia et al. (2005), (48) Aleksandrovich et al. (1995), (49) Cornelisse et al. (2006), (50) Bikmaev et al. (2006b), (51) Chernyakova et al. (2005b), (52) Reig et al. (2005), (53) Hannikainen et al. (2003), (54) Sunyaev et al. (2003b), (55) Burenin et al. (2006b), (56) Negueruela et al. (2005), (57) Keek et al. (2006), (58) Krivonos et al. (2005b), (59) Grebenev et al. (2004a), (60) Burenin et al. (2006a), (61) Grebenev et al. (2005b), (62) Kuiper et al. (2006), (63) Masetti et al. (2006a), (64) Lutovinov et al. (2004b), (65) Tueller et al. (2005), (66) Halpern (2006), (67) Masetti et al. (2006), (68) Masetti et al. (2005), (69) Karasev et al. (2007), (70) Brandt et al. (2006), (71) Chernyakova et al. (2003), (72) Gaensicke et al. (2005), (73) Turler et al. (2005), (74) Grebenev et al. (2005a), (75) Gotz et al. (2006), (76) Krivonos et al. (2006), (77) Sazonov et al. (2007), (78) Rea et al. (2006), (79) Bélanger et al. (2006), (80) Palmer et al. (2005), (81) Torres et al. (2005), (82) Chelovekov et al. (2006), (83) Tomsick et al. (2006), (84) Revnivtsev et al. (2003a), (85) Courvoisier et al. (2003), (86) Walter et al. (2003), (87) Tomsick et al. (2003), (88) Revnivtsev et al. (2003b), (89) Patel et al. (2004), (90) Bodaghee et al. (2006), (91) Tomsick et al. (2004), (92) Molkov et al. (2003), (93) Lutovinov et al. (2005b), (94) Kuulkers et al. (2003), (95) Revnivtsev et al. (2003c), (96) Lutovinov et al. (2003a), (97) Lutovinov et al. (2005c), (98) Revnivtsev et al. (2004c), (99) Augello et al. (2003), (100) Lutovinov et al. (2003b) (101) Sazonov et al., in preparation.

References

Aharonian, F., et al. 2006, A&A, 449, 223

Aleksandrovich, N. L., Aref'ev, V. A., Borozdin, K. N., Syunyaev, R. A., & Skinner, G. K. 1995, Astronomy Letters, 21, 431

Augello, G., Iaria, R., Robba, N., et al. 2003, ApJ, 596, L63

Bahcall N. A., Burgett W. S., 1986, ApJ, 300, L35

Barlow, E. J., Bird, A., Clark, D., et al. 2005, A&A, 437, L27

Barlow, E. J., Knigge, C., Bird, A. J., Dean, A. J., Clark, D. J., Hill, A. B., Molina, M., & Sguera, V. 2006, MNRAS, 372, 234

Bassani, L., De Rosa, A., Bazzano, A., Bird, A.J., Dean, A.J., Gehrels, N., et al., 2005, ApJ, 634, L21

Bassani, L., Molina, M., Malizia, A., et al., 2006, ApJ, 636, L65

Beckmann V., Soldi S., Shrader C. R., Gehrels N., Produit N., 2006, ApJ, 652, 126

Bélanger G., Goldwurm, A., Renaud, M., et al. 2006, ApJ, 636, 275

Bikmaev, I.F., Sunyaev, R.A., Revnivtsev, M.G., & Burenin, R.A., 2006a, Astron. Lett., 32, 221

Bikmaev, I.F., Sunyaev, R.A., Revnivtsev, M.G., & Burenin, R.A., 2006b, Astron. Lett., 32, 588

Bird, A. J., Barlow, E. J., Bassani, L., et al. 2006, ApJ, 636, 765

Bird A. J.,Malizia A., Bazzano A., Barlow E. J., Bassani L., Hill A. B., Belanger G., Capitanio F., et al. 2006, astro, arXiv:astro-ph/0611493

Bodaghee, A., Walter, R., Zurita Heras, J., et al. 2006, A&A, 447, 1027

Brandt, S., Kuulkers, E., Bazzano, A., et al. 2005, Astron. Telegram, 622, 1

Brandt, S., Budtz-Jørgensen, C., & Chenevez, J. 2006, Astron. Telegram, 778, 1

Burenin, R., Mescheryakov, A., Revnivtsev, M., Bikmaev, I., & Sunyaev, R. 2006a, The Astronomer's Telegram, 880, 1

Burenin, R., Mescheryakov, A., Sazonov, S., Revnivtsev, M., Bikmaev, I., & Sunyaev, R. 2006b, Astron. Telegram, 883, 1

Bykov, A., Krassilshchikov, A., Uvarov, Yu., et al. 2004, A&A, 427, L21

Bykov, A., Krassilshchikov, A., Uvarov, Yu., et al. 2006, ApJ, 649, L21

Chelovekov, I., Grebenev, S., Sunyaev, R. 2006, Astronomy Letters, 32, 456

Chernyakova, M., Lutovinov, A., Capitanio, F., Lund, N., & Gehrels, N. 2003, Astron. Telegram, 157, 1

Chernyakova, M., Courvoisier, T., Rodriguez, J., Lutovinov, A. 2005a, Astron. Telegram, 519, 1

Chernyakova, M., Lutovinov, A., Rodríguez, J., & Revnivtsev, M. 2005b, MNRAS, 364, 455

Cornelisse, R., Charles, P. A., & Robertson, C. 2006, MNRAS, 366, 918

Courvoisier, T., Walter, R., Rodriguez, J., Bouchet, L., Lutovinov A. 2003, IAUC 8063, 1

Crawford, D. F., Jauncey, D. L., & Murdoch, H. S. 1970, ApJ, 162, 405

Donato, D., Sambruna, R.M., & Gliozzi, M., 2005, A&A, 433, 1163

Davis M., Peebles P. J. E., 1983, ARA&A, 21, 109

den Hartog, P., Hermsen, W., Kuiper, L., et al. 2004a, Astron. Telegram, 261, 1

den Hartog, P., Kuiper, L., Corbet, R., et al. 2004b, Astron. Telegram, 281, 1

den Hartog, P., Kuiper, L., Hermsen, W., et al. 2005, Astron. Telegram, 394, 1

Hopkins, P. F., Hernquist, L., Cox, T. J., Di Matteo, T., Robertson, B., & Springel, V. 2006, ApJS, 163, 1

Fenimore, E. E., Cannon T. M., 1981 Applied Optics, 20, 1858.

Forman, W., Jones, C., Cominsky, L., Julien, P., Murray, S., Peters, G., Tananbaum, H., & Giacconi, R. 1978, ApJS, 38, 357

Fouqué, P., Solanes, J. M., Sanchis, T., & Balkowski, C. 2001, A&A, 375, 770
Gaensicke, B. T., Marsh, T. R, Edge, A., et al. 2005, Astron. Telegram, 463, 1
Górski, K. M., Hivon, E., Banday, A. J., Wandelt, B. D., Hansen, F. K., Reinecke, M., & Bartelmann, M. 2005, ApJ, 622, 759
Gotz, D., Schanne, S., Rodriguez, J., Leyder, J.-C., von Kienlin, A., Mowlavi, N., & Mereghetti, S. 2006, Astron. Telegram, 813, 1
Grebenev, S. A., Ubertini, P., Chenevez, J., Orr, A., & Sunyaev, R. A. 2004a, Astron. Telegram, 275, 1
Grebenev, S., Ubertini, P., Chenevez, J., et al. 2004b, Astron. Telegram, 350, 1
Grebenev, S. A., Molkov, S. V., & Sunyaev, R. A. 2005a, Astron. Telegram, 467, 1
Grebenev, S. A., Molkov, S. V., & Sunyaev, R. A. 2005b, The Astronomer's Telegram, 616, 1
Grimm, H.-J., Gilfanov, M., & Sunyaev, R. 2002, A&A, 391, 923
Gros, A., Goldwurm, A., Cadolle-Bel, M., Goldoni, P., Rodriguez, J., Foschini, L., Del Santo, M., & Blay, P. 2003, A&A, 411, L179
Halpern, J. P. 2006, Astron. Telegram, 847, 1
Hannikainen, D., Rodriguez, J., Pottschmidt, K. et al. 2003, IAUC 8088, 1
Hanski, M. O., Theureau, G., Ekholm, T., & Teerikorpi, P. 2001, A&A, 378, 345
in't Zand, J. J. M., & Heise, J. 2004, Astron. Telegram, 362, 1
in't Zand, J. J. M. 2005, A&A, 441, L1
Karasev, D., Lutovinov, A., Grebenev, S. 2007, Astronomy Letters, 33, 135
Keek, S., Kuiper, L., & Hermsen, W. 2006, The Astronomer's Telegram, 810, 1
Kocevski D. D., Ebeling H., 2006, ApJ, 645, 1043
Kormendy, J. 2001, Revista Mexicana de Astronomia y Astrofisica Conference Series, 10, 69
Kormendy, J., & Richstone, D. 1995, ARA&A, 33, 581
Koyama, K., Petre, R., Gotthelf, E. V., Hwang, U., Matsuura, M., Ozaki, M., & Holt, S. S. 1995, Nature, 378, 255
Koyama, K., Kinugasa, K., Matsuzaki, K., Nishiuchi, M., Sugizaki, M., Torii, K., Yamauchi, S., & Aschenbach, B. 1997, PASJ, 49, L7
Kretschmar, P., Mereghetti, S., Hermsen, W., et al. 2004, Astron. Telegram, 345, 1
Krivonos, R., Vikhlinin, A., Churazov, E., Lutovinov, A., Molkov, S., & Sunyaev, R., 2005a, ApJ, 625, 89
Krivonos, R., Molkov, S., Revnivtsev, M., Grebenev, S., Sunyaev, R., & Paizis, A. 2005b, Astron. Telegram, 545, 1
Krivonos, R., Revnivtsev, M., Sazonov, S., Churazov, E., & Sunyaev, R. 2006, IAU Symposium, 230, 455
Krivonos, R., Revnivtsev, M., Churazov, E., et al. 2006, A&A, accepted (astro-ph/0605420)
Kuiper, L., Keek, S., Hermsen, W., Jonker, P. G., & Steeghs, D. 2006, Astron. Telegram, 684, 1
Kuulkers, E., Lutovinov, A., Parmar, A., et al. 2003, Astron. Telegram, 149, 1
Kuulkers, E., Shaw, S., Paizis, A., et al. 2006, Astron. Telegram, 874, 1
Lahav, O., Lynden-Bell, D., & Rowan-Robinson, M. 1988, MNRAS, 234, 677
Lahav, O., Fabian, A. C., Edge, A. C., & Putney, A. 1989, MNRAS, 238, 881
Levine, A. M., et al. 1984, ApJS, 54, 581
Liu, Q. Z., van Paradijs, J., & van den Heuvel, E. P. J. 2000, A&AS, 147, 25
Liu, Q. Z., van Paradijs, J., & van den Heuvel, E. P. J. 2001, A&A, 368, 1021
Lubinski, P., Gadolle Bel, M., von Kienlin, A., et al. 2005, Astron. Telegram, 469, 1
Lutovinov, A. A., & Revnivtsev, M. G. 2003, Astronomy Letters, 29, 719
Lutovinov, A., Walter, R., Belanger, R., et al. 2003a, Astron. Telegram, 155, 1
Lutovinov, A., Shaw, S., Foschini, L., Paul, J. 2003b, Astron. Telegram, 154, 1
Lutovinov, A., Rodriguez, J., Produit, N., Paul, J. 2003c, Astron. Telegram, 151, 1
Lutovinov, A., Rodriguez, J., Budtz-Jorgensen, C., et al. 2004a, Astron. Telegram, 329, 1
Lutovinov, A., Bel, M. C., Belanger, G., Goldwurm, A., Budtz-Jorgensen, C., Mowlavi, N., Paul, J., & Orr, A. 2004, Astron. Telegram, 328, 1
Lutovinov, A., Rodriguez, J., Revnivtsev, M., & Shtykovskiy, P. 2005a, A&A, 433, L41
Lutovinov, A., Revnivtsev, M., Gilfanov, M., et al. 2005b, A&A, 444, 821
Lutovinov, A., Revnivtsev, M., Molkov, S., Sunyaev, R. 2005c, A&A, 430,997
Lynden-Bell, D., Faber, S. M., Burstein, D., Davies, R. L., Dressler, A., Terlevich, R. J., & Wegner, G. 1988, ApJ, 326, 19
Malizia, A., Bassani, L., Stephen, J., et al. 2005, ApJ, 630, L157
Masetti, N., Palazzi, E., Bassani, L., Malizia, A., & Stephen, J.B., 2004, A&A, 426, L41
Masetti, N., Bassani, L., Bird, A., Bassano, A. 2005, Astron. Telegram, 528,1
Masetti, N., Morelli, L., Palazzi, E., Stephen, J., Bazzano, A., Dean, A. J., Walter, R., & Minniti, D. 2006a, Astron. Telegram, 783, 1
Masetti, N., Morelli, L., Palazzi, E., Galaz, G., Bassani, L., Bazzano, A., et al., 2006b, A&A, 459, 21
Masetti, N., Pretorius, M.L., Palazzi, E., Bassani, L., Bazzano, A., & Bird, A.J, 2006c, A&A, 449, 1139
Masetti, N., Bassani, L., Dean, A. J., Ubertini, P., & Walter, R. 2006d, The Astronomer's Telegram, 715, 1
Masetti, N., Bassani, L., Bazzano, A., Bird, A.J., Dean, A.J., Malizia, A., et al., 2006e, A&A, 455, 11
Miyaji, T., & Boldt, E. 1990, ApJ, 353, L3
Molkov, S., Mowlavi, N., Goldwurm, A., et al. 2003, Astron. Telegram, 176, 1

Molkov S. V., Cherepashchuk A. M., Lutovinov A. A., Revnivtsev M. G., Postnov K. A., Sunyaev R. A., 2004, AstL, 30, 534
Morelli, L., Masetti, N., Bassani, L., et al., 2006, Astron. Telegram, 785, 1
Negueruela, I., Smith, D., Chaty, S. 2005, Astron. Telegram, 470, 1
Negueruela, I., & Smith, D. 2006, Astron. Telegram, 831, 1
Neronov A., Chernyakova M., Courvoisier T. J. -., Walter R., 2005, astro, arXiv:astro-ph/0506437
Palmer, D. M., Barthelmey, S. D., Cummings, J. R., Gehrels, N., Krimm, H. A., Markwardt, C. B., Sakamoto, T., & Tueller, J. 2005, The Astronomer's Telegram, 546, 1
Patel, S., Kouveliotou, C., Tennant, A., et al. 2004, ApJ, 602, L45
Pavlinskii, M. N., Grebenev, S. A., & Syunyaev, R. A. 1992, Soviet Astronomy Letters, 18, 88
Pfeffermann, E., & Aschenbach, B. 1996, Roentgenstrahlung from the Universe, 267
Plionis, M., & Kolokotronis, V. 1998, ApJ, 500, 1
Produit, N., Ballet, J., Mowlavi, N. 2003, Astron. Telegram., 278, 1
Protheroe, R. J., Wolfendale, A. W., & Wdowczyk, J. 1980, MNRAS, 192, 445
Rea, N., Testa, V., Israel, G., et al. 2006, Astron. Telegram, 713, 1
Rees M. J., 1980, IAUS, 92, 207
Reig, P., Negueruela, I., Papamastorakis, G., Manousakis, A., & Kougentakis, T. 2005, A&A, 440, 637
Renaud, M., Gros, A., Lebrun, F., Terrier, R., Goldwurm, A., Reynolds, S., & Kalemci, E. 2006a, A&A, 456, 389
Renaud, M., Bélanger, G., Paul, J., Lebrun, F., & Terrier, R. 2006b, A&A, 453, L5
Revnivtsev, M. G., Sazonov, S. Y., Gilfanov M. R., Sunyaev, R. A. 2003a, Astronomy Letters, 29, 587
Revnivtsev, M., Tuerler, M., Del Santo, M., et al. 2003b, IAUC 8097, 1
Revnivtsev, M., Chernyakova, M., Capitanio, F., et al. 2003c, Astron. Telegram, 132, 1
Revnivtsev, M., Sazonov, S., Jahoda, K., & Gilfanov, M., 2004a, A&A, 418, 927
Revnivtsev, M. G., Sunyaev, R. A., Gilfanov, M. R., Churazov, E. M., Goldwurm, A., Paul, J., Mandrou, P., & Roques, J. P. 2004, Astronomy Letters, 30, 527
Revnivtsev, M., Sazonov, S., Churazov, E., et al. 2004b, A&A, 425, L49
Revnivtsev, M., Sunyaev, R., Varshalovich, D., et al. 2004c, Astronomy Letters, 30, 382
Revnivtsev, M. G., Sazonov, S. Y., Molkov, S. V., Lutovinov, A. A., Churazov, E. M., & Sunyaev, R. A. 2006, Astronomy Letters, 32, 145
Richstone, D., et al. 1998, Nature, 395, A14
Rodriguez, J., Domingo Garau, A., Grebenev, S., et al. 2004, Astron. telegram, 340, 1
Rodriguez, J., Cabanac, C., Hannikainen, D. C., Beckmann, V., Shaw, S. E., & Schultz, J. 2005, A&A, 432, 235
Rowan-Robinson M., et al., 2000, MNRAS, 314, 375
Saunders, W., et al. 2000, MNRAS, 317, 55
Sazonov, S., Churazov, E., Revnivtsev, M., Vikhlinin, A., & Sunyaev, R., 2005, A&A, 444, L37
Sazonov, S., Revnivtsev, M., Krivonos, R., Churazov, & Sunyaev, R., 2006, A&A, 462, 57
Sguera, V., Bazzano, A., Bird, A., et al. 2006, ApJ, 646, 452
Skinner, G. K. et al. 1987, Astroph.Sp.Sci., 136, 337-349.
Smith, D. M., Heindl, W. A., Markwardt, C. B., Swank, J. H., Negueruela, I., Harrison, T. E., & Huss, L. 2006, ApJ, 638, 974
Slane, P., Gaensler, B. M., Dame, T. M., Hughes, J. P., Plucinsky, P. P., & Green, A. 1999, ApJ, 525, 357
Sunyaev, R., Lutovinov, A., Molkov, S., Deluit, S. 2003a, Astron. Telegram, 181, 1
Sunyaev, R., Grebenev, S., Lutovinov, A., et al. 2003b, Astron. Telegram, 192, 1
Tonry, J. L., Blakeslee, J. P., Ajhar, E. A., & Dressler, A. 2000, ApJ, 530, 625
Tomsick, J., Lingenfelter, R., Walter, R., et al. 2003, IAUC 8076, 1
Tomsick, J., Lingenfelter, R., Corbel, S., Goldwurm, A., Kaaret, P. 2004, Astron. Telegram, 224, 1
Tomsick, J., Chaty, S., Rodriguez, J., et al. 2006, ApJ, 647, 1309
Toor, A., & Seward, F. D. 1974, AJ, 79, 995
Torres, M. A. P., et al. 2005, Astron. Telegram, 551, 1
Tueller, J., Barthelmy, S., Burrows, D., et al. 2005, Astron. Telegram, 669, 1
Turler, M., Bel, M. C., Diehl, R., Westergaard, N.-J., McBreen, B., Williams, O. R., Grebenev, S. A., & Lutovinov, A. 2005, The Astronomer's Telegram, 624, 1
Ubertini P., et al., 2003, A&A, 411, L131
Ubertini, P., Bassani, L., Malizia, A., et al. 2005, ApJ, 629, L109
Walter, R., Bodaghee, A., Barlow, E., et al. 2003, Astron. Telegram, 229, 1
Walter, R., Zurita Heras, J., Bassani, L., et al. 2006, A&A, 453, 133
Winkler, C., Courvoisier, T., Di Cocco, G., et al. 2003, A&A, 411, L1

Table 1. INTEGRAL Catalog

Id	Name	RA	Dec	$F_{17-60\ \mathrm{keV}}$	Type	Counterpart	Notes
1	IGR J00234+6141	5.723	61.700	0.38 ± 0.10	CV		43,50
2	TYCHO SNR	6.334	64.150	0.64 ± 0.10	SNR		
3	V709 Cas	7.205	59.300	3.91 ± 0.11	CV		36
4	IGR J00291+5934	7.254	59.563	4.01 ± 0.11	LMXB		
5	87GB003300.9+593328	8.977	59.827	0.72 ± 0.11	AGN		1
6	IGR J00370+6122	9.286	61.386	0.60 ± 0.11	HMXB		45
7	MRK 348	12.181	31.947	5.18 ± 0.58	AGN	NGC 262	
8	1WGA J0053.8-722	13.526	-72.468	2.36 ± 0.38	HMXB		
9	Gamma Cas	14.176	60.712	3.17 ± 0.12	Star		
10	SMC X-1	19.299	-73.449	30.54 ± 0.36	HMXB		
11	1A 0114+650	19.516	65.289	7.64 ± 0.14	HMXB		
12	4U 0115+63	19.625	63.746	2.01 ± 0.14	HMXB		
13	NGC 0526A	20.951	-34.925	3.84 ± 0.81	AGN		
14	IGR J01363+6610	24.060	66.188	$15.61 \pm 2.20^{\mathrm{R185}}$	HMXB		59,52
15	RX J0137.7+5814	24.443	58.221	0.77 ± 0.20			
16	ESO 297- G 018	24.639	-40.020	$3.85 \pm 0.80^{\mathrm{R374}}$	AGN		
17	4U 0142+61	26.630	61.738	2.02 ± 0.19	AXP		
18	RJ 0146.9+6121	26.744	61.351	2.57 ± 0.20	HMXB		
19	IGR J01528-0326	28.208	-3.450	1.14 ± 0.21	AGN	MCG -01-05-047	55
20	NGC 788	30.277	-6.819	3.37 ± 0.20	AGN		
21	IGR J02095+5226	32.392	52.458	2.76 ± 0.50	AGN	LEDA 138501 1ES 0206+522	
22	MRK 1040	37.063	31.316	3.39 ± 0.57	AGN	NGC 931	
23	IGR J02343+3229	38.599	32.475	2.71 ± 0.44	AGN	NGC 973 IRAS 02313+3217	55
24	NGC 1052	40.267	-8.236	1.48 ± 0.30	AGN		
25	NGC 1068	40.687	-0.010	1.32 ± 0.21	AGN		
26	4U 0241+61	41.262	62.464	3.32 ± 0.42	AGN		
27	IGR J02466-4222	41.644	-42.360	2.16 ± 0.38	AGN?	MCG -07-06-018	77,101
28	IGR J02524-0829	43.115	-8.486	2.20 ± 0.47	AGN?	MCG-02-08-014	
29	NGC 1142	43.804	-0.186	3.22 ± 0.25	AGN	NGC 1144	
30	PERSEUS CLUSTER[a]	49.973	41.509	2.49 ± 0.24	Cluster		
31	1H 0323+342	51.140	34.168	1.91 ± 0.33	AGN		
32	GK Per	52.777	43.880	1.82 ± 0.27	CV		
33	IGR J03334+3718	53.362	37.313	1.37 ± 0.29	AGN		60,77
34	NGC 1365	53.428	-36.170	2.30 ± 0.46	AGN		
35	V 0332+53	53.751	53.172	135.14 ± 0.44	HMXB		
36	4U 0352+30	58.849	31.036	36.69 ± 0.62	HMXB	X Per	
37	3C111	64.581	38.013	5.47 ± 0.61	AGN		
38	LEDA 168563	73.044	49.531	3.09 ± 0.78	AGN	1RXS J045205.0+493248	
39	ESO 033-G002	74.001	-75.538	1.36 ± 0.19	AGN		
40	IGR J05007-7047	75.203	-70.775	1.18 ± 0.17	HMXB	IGR J05009-7044	2
41	V1062 Tau	75.617	24.732	$3.67 \pm 0.62^{\mathrm{R102}}$	CV		
42	IRAS 05078+1626	77.705	16.513	4.14 ± 0.53	AGN		
43	4U 0513-40	78.534	-40.069	3.39 ± 0.60	LMXB		
44	AKN 120	79.026	-0.140	5.86 ± 2.46	AGN		
45	IGR J05305-6559[b]	82.636	-65.984	1.72 ± 0.34			
46	LMC X-4	83.210	-66.367	15.95 ± 0.17	HMXB		
47	Crab	83.632	22.016	1000.00 ± 0.41	PSR		
48	TW Pic	83.689	-57.988	0.97 ± 0.27	CV		
49	A 0535+262	84.735	26.324	3.45 ± 0.42	HMXB		
50	LMC X-1	84.912	-69.748	3.72 ± 0.17	HMXB		
51	PSR 0540-69	85.005	-69.338	1.70 ± 0.17	PSR		
52	BY Cam	85.713	60.868	2.48 ± 0.51	CV		36
53	MCG 8-11-11	88.801	46.437	3.92 ± 1.05	AGN		
54	IRAS 05589+2828	90.601	28.461	3.38 ± 0.71	AGN		
55	ESO 005- G 004	92.575	-86.554	1.76 ± 0.32	AGN		
56	MRK 3	93.908	71.036	4.77 ± 0.21	AGN		
57	4U 0614+091	94.282	9.139	20.81 ± 0.67	LMXB		
58	IGR J06239-6052[b]	95.936	-60.974	1.16 ± 0.22			
59	MRK 6	103.048	74.423	2.55 ± 0.21	AGN		
60	IGR J07264-3553	111.595	-35.900	1.89 ± 0.42	AGN	LEDA 096373	
61	EXO 0748-676	117.146	-67.754	19.32 ± 0.35	LMXB		
62	IGR J07563-4137	119.055	-41.638	0.86 ± 0.17	AGN	IGR J07565-4139 2MASX J07561963-4137420	44,2
63	IGR J07597-3842	119.934	-38.727	2.03 ± 0.18	AGN		13,8
64	ESO 209-G012	120.496	-49.734	1.16 ± 0.17	AGN		
65	IGR J08023-6954	120.762	-69.924	3.70 ± 0.96			23
66	PG 0804+761	122.952	76.102	2.01 ± 0.43	AGN		
67	Vela pulsar	128.835	-45.182	7.03 ± 0.12	PSR		
68	4U 0836-429	129.354	-42.894	29.46 ± 0.12	LMXB		
69	FAIRALL 1146	129.621	-35.983	1.14 ± 0.17	AGN		
70	IGR J08408-4503	130.218	-45.056	0.33 ± 0.12	HMXB		75
71	S5 0836+71	130.340	70.902	2.43 ± 0.23	AGN		1
72	Vela X-1	135.531	-40.555	187.16 ± 0.14	HMXB		

Table 1 (cont'd)

Id	Name	RA	Dec	$F_{17-60\ \mathrm{keV}}$	Type	Counterpart	Notes
73	IGR J09026-4812	135.648	-48.221	1.32 ± 0.13			44
74	IRAS 09149-6206	139.043	-62.330	1.44 ± 0.18	AGN		
75	X 0918-548	140.102	-55.196	3.34 ± 0.15	LMXB		
76	SWIFT J0920.8-0805	140.213	-8.086	2.51 ± 0.70	AGN	MCG-01-24-012	
77	IGR J09251+5219	141.274	52.331	4.09 ± 0.79	AGN	Mrk 110	
78	IGR J09446-2636[c]	146.124	-26.628	2.73 ± 0.52	AGN	1RXS J094436.5-263353 6dF J0944370-263356	
79	NGC 2992	146.431	-14.335	3.55 ± 0.27	AGN		
80	MCG-5-23-16	146.916	-30.947	6.82 ± 0.59	AGN	ESO 434-G040	
81	IGR J09522-6231	148.025	-62.523	0.82 ± 0.15			77
82	NGC 3081	149.859	-22.816	3.23 ± 0.39	AGN		
83	IGR J10095-4248	152.449	-42.800	1.50 ± 0.27	AGN	ESO 263-G013	
84	GRO J1008-57	152.447	-58.298	4.11 ± 0.12	HMXB		
85	IGR J10100-5655	152.529	-56.914	1.20 ± 0.13	HMXB		62,8
86	IGR J10109-5746	152.753	-57.795	1.01 ± 0.13	SimbStar?	2RXP J101103.0-574810	23,67
87	NGC 3227	155.876	19.867	6.32 ± 0.58	AGN		
88	IGR J10252-6829	156.287	-68.460	3.14 ± 0.87			23
89	NGC 3281	157.935	-34.855	2.70 ± 0.45	AGN		
90	3U 1022-55	159.401	-56.801	$4.11 \pm 0.47^{\mathrm{R85}}$	HMXB		
91	IGR J10386-4947	159.676	-49.789	1.03 ± 0.17	AGN	SWIFT J1038.8-4942	20
92	IGR J10404-4625	160.124	-46.391	1.47 ± 0.24	AGN	LEDA 93974	44,4
93	η Car	161.189	-59.719	0.68 ± 0.12	Star		
94	IGR J11085-5100	167.144	-51.014	0.19 ± 0.17			23
95	Cen X-3	170.306	-60.628	52.23 ± 0.13	HMXB		
96	IGR J11215-5952	170.429	-59.869	1.09 ± 0.13	HMXB		12,56
97	IGR J11305-6256	172.779	-62.945	3.45 ± 0.14	XRB		34,4
98	IGR J11321-5311	173.047	-53.200	22.36 ± 2.14			58
99	NGC 3783	174.739	-37.766	8.58 ± 1.30	AGN		
100	IGR J11395-6520	174.858	-65.406	$10.68 \pm 0.86^{\mathrm{R88}}$	RS CVn?	HD 101379	
101	IGR J11435-6109	176.031	-61.106	0.88 ± 0.15	HMXB		14,18
102	A 1145.1-6141	176.870	-61.956	22.91 ± 0.15	HMXB		
103	4U 1145-619[b]	177.000	-62.207	3.57 ± 0.15	HMXB		
104	IGR J12026-5349	180.686	-53.823	1.70 ± 0.21	AGN	WKK0560	23,2
105	NGC 4051	180.781	44.525	2.11 ± 0.48	AGN		
106	NGC 4138	182.352	43.672	1.67 ± 0.34	AGN		
107	NGC 4151	182.634	39.408	33.11 ± 0.30	AGN		
108	1ES 1210-646	183.269	-64.917	0.66 ± 0.18			
109	IGR J12143+2933	183.597	29.561	0.67 ± 0.25	AGN	WAS 49B	
110	NGC 4253	184.592	29.825	1.07 ± 0.21	AGN		
111	NGC 4258	184.747	47.309	1.33 ± 0.39	AGN		
112	PKS 1219+04	185.588	4.230	0.91 ± 0.16	AGN		
113	MRK 50	185.860	2.676	0.91 ± 0.16	AGN		
114	NGC 4388	186.444	12.664	12.50 ± 0.21	AGN		
115	NGC 4395	186.462	33.565	1.08 ± 0.20	AGN		
116	GX 301-2	186.651	-62.772	122.97 ± 0.19	HMXB		
117	XSS J12270-4859	186.978	-48.907	1.39 ± 0.33	CV		63
118	3C273	187.271	2.050	9.66 ± 0.16	AGN		
119	IGR J12349-6434	188.724	-64.565	3.56 ± 0.19	SimbStar?	RT Cru	17,68
120	NGC 4507	188.908	-39.905	7.64 ± 0.34	AGN		
121	IGR J12391-1612	189.792	-16.186	2.10 ± 0.43	AGN	LEDA 170194 XSS 12389-1614	23,2
122	NGC 4593	189.910	-5.347	4.09 ± 0.18	AGN		
123	WKK 1263	190.356	-57.841	0.89 ± 0.22	AGN		
124	PKS 1241-399	191.057	-40.115	1.24 ± 0.28	AGN		
125	4U 1246-588	192.386	-59.090	2.36 ± 0.21	HMXB?		40
126	3C279	194.030	-5.779	1.05 ± 0.19	AGN		
127	2S 1254-690	194.392	-69.296	2.60 ± 0.24	LMXB		41
128	Coma	194.865	27.938	1.58 ± 0.15	Cluster		
129	1RXP J130159.6-635806[b]	195.495	-63.969	1.64 ± 0.20	HMXB		51
130	PSR B1259-63[b]	195.699	-63.836	1.01 ± 0.19	HMXB		
131	MRK 783	195.741	16.361	0.86 ± 0.22	AGN		
132	IGR J13038+5348	195.951	53.798	2.19 ± 0.46	AGN	MCG+09-21-096	60,77
133	NGC 4945	196.364	-49.470	13.92 ± 0.25	AGN		
134	ESO 323-G077	196.607	-40.423	1.94 ± 0.24	AGN		
135	IGR J13091+1137	197.270	11.619	2.44 ± 0.29	AGN	NGC 4992	23,2
136	IGR J13109-5552	197.689	-55.865	1.29 ± 0.21		PMN J1310-5552	23
137	NGC 5033	198.350	36.572	0.84 ± 0.19	AGN		
138	IGR J13149+4422[c]	198.743	44.389	1.51 ± 0.27	AGN	Mrk 248	
139	Cen A	201.363	-43.019	39.19 ± 0.22	AGN		
140	4U 1323-619	201.643	-62.136	5.28 ± 0.18	LMXB		
141	IGR J13290-6323[c]	202.268	-63.392	$2.30 \pm 0.37^{\mathrm{R92}}$			
142	ESO 383-G018	203.332	-34.030	1.22 ± 0.27	AGN		
143	BH CVn	203.699	37.182	0.57 ± 0.26	RS CVn		
144	MCG-6-30-15	203.990	-34.288	2.53 ± 0.26	AGN	ESO 383-G035	
145	NGC 5252	204.564	4.528	3.45 ± 1.03	AGN		

Table 1 (cont'd)

Id	Name	RA	Dec	$F_{17-60\ \mathrm{keV}}$	Type	Counterpart	Notes
146	MRK 268	205.420	30.395	1.22 ± 0.21	AGN		
147	4U 1344-60	206.894	-60.615	4.16 ± 0.17	AGN		
148	IC 4329A	207.333	-30.309	11.28 ± 0.36	AGN		
149	IGR J14003-6326	210.204	-63.414	0.89 ± 0.15			57
150	V834 Cen	212.196	-45.382	4.11 ± 0.91	CV		
151	Circinus galaxy	213.290	-65.342	13.11 ± 0.18	AGN		
152	NGC 5506	213.312	-3.220	9.32 ± 0.46	AGN		
153	IGR J14175-4641	214.296	-46.671	0.91 ± 0.19	AGN		23,8
154	NGC 5548	214.541	25.155	1.44 ± 0.35	AGN		
155	ESO 511-G030	214.885	-26.633	2.32 ± 0.63	AGN		
156	IGR J14298-6715	217.388	-67.251	0.89 ± 0.18			57
157	IGR J14331-6112	218.273	-61.221	1.00 ± 0.15			57
158	IGR J14471-6414	221.528	-64.284	0.86 ± 0.15			57
159	IGR J14471-6319	221.834	-63.289	0.66 ± 0.16	AGN		23,8
160	IGR J14493-5534	222.311	-55.589	1.15 ± 0.16	AGN	2MASX J14491283-5536194	22,9
161	IGR J14515-5542	222.887	-55.691	1.08 ± 0.15	AGN	WKK 4374	62,8
162	IGR J14536-5522	223.421	-55.363	1.20 ± 0.16	CV		62,63
163	IGR J14552-5133	223.846	-51.571	0.98 ± 0.16	AGN	WKK 4438	23,8
164	IGR J14561-3738[c]	224.055	-37.632	0.98 ± 0.18	AGN	ESO 386- G 034	101
165	IC 4518A	224.427	-43.125	1.70 ± 0.16	AGN		
166	IGR J15094-6649	227.382	-66.816	1.05 ± 0.21	CV		23,63
167	PSR 1509-58	228.480	-59.145	8.85 ± 0.15	PSR		
168	4U 1516-569	230.167	-57.168	7.64 ± 0.15	LMXB		
169	IGR J15360-5750	234.014	-57.806	0.93 ± 0.15			23
170	4U 1538-522	235.600	-52.385	16.42 ± 0.13	HMXB		
171	XTE J1543-568	236.011	-56.748	0.84 ± 0.14	HMXB		
172	4U 1543-624	236.964	-62.578	2.27 ± 0.18	LMXB		
173	NY Lup	237.052	-45.472	4.10 ± 0.14	CV	1RXS J154814.5-452845	
174	XTE J1550-564	237.751	-56.474	28.65 ± 0.14	LMXB		
175	IGR J15539-6142	238.468	-61.676	0.85 ± 0.17			57
176	4U 1556-605	240.363	-60.716	0.84 ± 0.16	LMXB		
177	WKK 6092	242.981	-60.637	1.16 ± 0.17	AGN		
178	4U 1608-522	243.177	-52.425	6.48 ± 0.13	LMXB		
179	IGR J16167-4957	244.162	-49.975	1.45 ± 0.14	CV	1RXS J161637.2-495847	86,36
180	IGR J16175-5059	244.357	-50.972	0.60 ± 0.13	PSR	PSR J1617-5055	
181	IGR J16185-5928	244.635	-59.468	1.21 ± 0.16	AGN	WKK 6471	23,8
182	IGR J16195-4945	244.893	-49.755	1.80 ± 0.14	HMXB	AX J161929-4945	86,83
183	IGR J16195-2807	244.871	-28.151	2.07 ± 0.31	RS CVn?	1RXS J161933.6-280736	44
184	Sco X-1	244.981	-15.637	581.08 ± 0.44	LMXB		
185	IGR J16207-5129	245.194	-51.505	3.01 ± 0.14	HMXB		86,83
186	SWIFT J1626.6-5156	246.659	-51.938	$23.58 \pm 1.88^{\mathrm{R399}}$	LMXB		78
187	4U 1624-49	247.002	-49.209	3.88 ± 0.14	LMXB		
188	IGR J16318-4848	247.953	-48.819	19.53 ± 0.14	HMXB		84,85
189	IGR J16320-4751	248.013	-47.876	15.34 ± 0.14	HMXB	AX J1631.9-4752	87,25
190	4U 1626-67	248.076	-67.466	13.58 ± 0.34	LMXB		
191	4U 1630-47	248.503	-47.391	44.73 ± 0.14	LMXB		
192	ESO 137-G34	248.790	-58.088	1.18 ± 0.16	AGN		
193	IGR J16358-4726[b]	248.992	-47.407	1.42 ± 0.13	HMXB		88,89
194	AX J163904-4642	249.768	-46.707	3.95 ± 0.13	HMXB		90
195	4U 1636-536	250.230	-53.751	38.18 ± 0.14	LMXB		
196	IGR J16418-4532	250.465	-45.534	3.50 ± 0.14	HMXB		91,37
197	GX 340+0	251.449	-45.616	28.85 ± 0.14	LMXB		
198	IGR J16465-4507[b]	251.648	-45.118	1.66 ± 0.14	HMXB		11,93
199	IGR J16479-4514	252.015	-45.207	3.41 ± 0.14	HMXB		92,93
200	IGR J16482-3036	252.058	-30.591	1.82 ± 0.17	AGN	2MASX J16481523-3035037	44,4
201	PSR J1649-4349	252.373	-43.823	2.24 ± 0.15	PSR		
202	IGR J16500-3307	252.493	-33.113	1.12 ± 0.16		1RXS J164955.1-330713	44
203	NGC 6221	253.120	-59.215	1.33 ± 0.19[e]	AGN		
204	NGC 6240	253.305	2.429	3.26 ± 0.97	AGN		
205	MKN 501	253.464	39.751	3.16 ± 0.30	AGN		
206	GRO J1655-40	253.499	-39.844	2.85 ± 0.14	LMXB		
207	IGR J16558-5203	254.032	-52.078	2.05 ± 0.15	AGN		86,8
208	IGR J16562-3301	254.073	-33.045	1.38 ± 0.14		SWIFT J1656.3-3302	
209	Her X-1	254.455	35.343	89.19 ± 0.28	LMXB		
210	AX J1700.2-4220	255.082	-42.335	1.17 ± 0.14	HMXB		63
211	OAO 1657-415	255.199	-41.656	63.72 ± 0.14	HMXB		
212	XTE J1701-462	255.232	-46.197	$39.26 \pm 2.50^{\mathrm{R407}}$	LMXB		
213	GX 339-4	255.705	-48.792	46.69 ± 0.15	LMXB		
214	4U 1700-377	255.984	-37.842	193.92 ± 0.14	HMXB		
215	GX 349+2	256.431	-36.421	40.74 ± 0.13	LMXB		
216	4U 1702-429	256.566	-43.037	14.93 ± 0.15	LMXB		
217	4U 1705-32	257.223	-32.322	1.93 ± 0.12	LMXB		
218	4U 1705-440	257.234	-44.102	25.00 ± 0.14	LMXB		
219	1RXS J170849.0-400910	257.214	-40.142	1.31 ± 0.14	AXP		
220	IGR J17091-3624	257.308	-36.408	5.35 ± 0.13	LMXB		94,24

Table 1 (cont'd)

Id	Name	RA	Dec	$F_{17-60\ \mathrm{keV}}$	Type	Counterpart	Notes
221	XTE J1709-267	257.386	-26.658	$13.92 \pm 0.67^{\mathrm{R171}}$	LMXB		
222	XTE J1710-281	257.549	-28.128	2.39 ± 0.12	LMXB		
223	RX J1713.7-3946	257.991	-39.862	0.61 ± 0.14	SNR	G347.3-0.5	
224	Oph cluster	258.114	-23.347	3.66 ± 0.13	Cluster		
225	SAX J1712.6-3739	258.153	-37.645	3.97 ± 0.13	LMXB		
226	4U 1708-40	258.120	-40.858	1.02 ± 0.14	LMXB		
227	V2400 Oph	258.149	-24.244	2.64 ± 0.13	CV		
228	KS 1716-389	259.003	-38.879	5.08 ± 1.23	HMXB	XTE J1716-389	48,49
229	NGC 6300	259.244	-62.830	3.29 ± 0.31	AGN		
230	IGR J17195-4100	259.911	-41.023	1.92 ± 0.14	CV	1RXS J171935.6-410054	86,36
231	XTE J1720-318	259.993	-31.753	2.59 ± 0.11	LMXB		
232	IGR J17200-3116	260.022	-31.294	1.86 ± 0.11	HMXB?	1RXS J172006.1-311702	86,8
233	IGR J17204-3554	260.087	-35.900	0.79 ± 0.12	AGN		44,27
234	EXO 1722-363	261.295	-36.282	8.18 ± 0.12	HMXB		
235	IGR J17254-3257	261.354	-32.953	1.57 ± 0.11	LMXB	1RXS J172525.5-325717	86,70
236	IGR J17269-4737	261.681	-47.647	$12.43 \pm 1.59^{\mathrm{R364}}$	XRB	XTE J1726-476	73
237	4U 1724-30	261.888	-30.804	17.09 ± 0.10	LMXB	Terzan 2	
238	IGR J17285-2922	262.163	-29.370	$3.68 \pm 0.57^{\mathrm{R120}}$	LMXB?	XTE J1728-295	86,35
239	IGR J17303-0601	262.579	-5.971	3.54 ± 0.30	CV	1RXS J173021.5-055933	86,72
240	GX 9+9	262.934	-16.952	11.08 ± 0.16	LMXB		
241	GX 354-0	262.988	-33.833	35.54 ± 0.10	LMXB		
242	GX 1+4	263.011	-24.747	54.39 ± 0.11	LMXB		
243	IGR J17320-1914	263.001	-19.195	1.14 ± 0.14	Nova	V2487 Oph	36
244	IGR J17331-2406	263.291	-24.142	1.24 ± 0.10			64
245	RapidBurster	263.349	-33.387	3.73 ± 0.11	LMXB		
246	IGR J17350-2045[c]	263.740	-20.754	0.90 ± 0.12			
247	IGR J17353-3539[c]	263.830	-35.663	0.80 ± 0.10			
248	IGR J17353-3257	263.848	-32.934	1.38 ± 0.10		IGR J17354-3255	22
249	IGR J17364-2711	264.117	-27.199	$1.60 \pm 0.30^{\mathrm{d}}$			82
250	GRS 1734-292	264.371	-29.139	5.18 ± 0.10	AGN		29
251	IGR J17379-3747[c]	264.465	-37.774	$6.34 \pm 0.91^{\mathrm{R165}}$			
252	SLX 1735-269	264.571	-26.991	10.00 ± 0.10	LMXB		
253	4U 1735-444	264.748	-44.453	25.07 ± 0.17	LMXB		
254	IGR J17391-3021	264.812	-30.355	1.08 ± 0.09	HMXB	XTE J1739-302	6,15
255	GRS 1736-297	264.899	-29.736	$4.99 \pm 0.52^{\mathrm{R409}}$			
256	XTE J1739-285[b]	264.975	-28.496	2.01 ± 0.10	LMXB		5
257	IGR J17402-3656	265.087	-36.936	0.87 ± 0.12	Open star cluster	NGC 6400	
258	SLX 1737-282[b]	265.168	-28.313	3.66 ± 0.09	LMXB		
259	IGR J17407-2808[b]	265.175	-28.133	1.47 ± 0.11	HMXB	2RXP J174040.9-280852	16,10
260	IGR J17419-2802[b]	265.485	-28.031	$8.11 \pm 0.10^{\mathrm{R409}}$			61
261	2E 1739.1-1210	265.484	-12.188	1.78 ± 0.20	AGN	IGR J17418-1212	
262	XTE J1743-363	265.753	-36.377	2.86 ± 0.11	HMXB?		10
263	1E 1740.7-294	265.976	-29.748	27.91 ± 0.09	LMXB		
264	IGR J17445-2747	266.082	-27.772	$4.39 \pm 0.67^{\mathrm{R165}}$			44
265	IGR J17448-3231[bc]	266.190	-32.528	0.56 ± 0.10			
266	KS 1741-293[b]	266.242	-29.337	5.11 ± 0.09	LMXB		
267	GRS 1741.9-2853[b]	266.250	-28.917	3.05 ± 0.09	LMXB		
268	IGR J17456-2901[b]	266.401	-29.026	5.61 ± 0.09		Nuclear stellar cluster	79,76
269	1E 1742.8-2853[b]	266.500	-28.914	5.95 ± 0.09	LMXB?		
270	A 1742-294	266.517	-29.508	11.82 ± 0.09	LMXB		
271	IGR J17464-3213	266.564	-32.237	32.30 ± 0.10	LMXB	H1743-322/XTE J1746-322	95
272	1E 1743.1-2843[b]	266.580	-28.735	5.45 ± 0.09	LMXB		
273	SAX J1747.0-2853[b]	266.761	-28.883	3.03 ± 0.09	LMXB		
274	SLX 1744-299/300[b]	266.834	-30.010	7.57 ± 0.09	LMXB		
275	IGR J17473-2721	266.841	-27.352	$5.14 \pm 0.73^{\mathrm{R304}}$			74
276	IGR J17475-2253[c]	266.901	-22.862	0.97 ± 0.10			
277	IGR J17475-2822	266.864	-28.364	2.51 ± 0.10	Molecular cloud	SgrB2	21
278	GX 3+1	266.983	-26.563	10.14 ± 0.10	LMXB		
279	A 1744-361	267.052	-36.133	$16.22 \pm 0.11^{\mathrm{R181}}$	LMXB		
280	4U 1745-203	267.217	-20.359	$12.03 \pm 0.54^{\mathrm{R120}}$	LMXB		
281	AX J1749.1-2733[b]	267.275	-27.550	1.48 ± 0.10	XRB?		10
282	IGR J17488-3253	267.223	-32.907	1.34 ± 0.10	AGN		86,8
283	AX J1749.2-2725[b]	267.292	-27.421	1.60 ± 0.09	HMXB		
284	SLX 1746-331	267.477	-33.201	0.82 ± 0.10	LMXB		
285	4U 1746-37	267.548	-37.046	2.95 ± 0.12	LMXB		
286	IGR J17505-2644[c]	267.636	-26.744	0.66 ± 0.10			
287	GRS 1747-313	267.689	-31.284	1.39 ± 0.09	LMXB	Terzan 6	
288	XTE J1751-305	267.816	-30.616	$5.91 \pm 0.61^{\mathrm{R299}}$	LMXB		
289	IGR J17513-2011	267.820	-20.184	1.62 ± 0.12	AGN		44,8
290	SWIFT J1753.5-0127	268.361	-1.452	3.44 ± 0.24	LMXB?		80,81
291	AX J1754.2-2754	268.495	-28.026	2.05 ± 0.53	LMXB		
292	IGR J17544-2619	268.619	-26.325	0.65 ± 0.09	HMXB		54,31
293	IGR J17585-3057[c]	269.636	-30.956	0.79 ± 0.09			
294	IGR J17597-2201	269.946	-22.026	5.61 ± 0.11	LMXB?	XTE J1759-220	96,97
295	GX 5-1	270.283	-25.075	45.54 ± 0.10	LMXB		

Table 1 (cont'd)

Id	Name	RA	Dec	$F_{17-60\ \mathrm{keV}}$	Type	Counterpart	Notes
296	GRS 1758-258	270.302	-25.743	54.32 ± 0.10	LMXB		
297	GX 9+1	270.385	-20.527	15.47 ± 0.12	LMXB		
298	IGR J18027-2016	270.666	-20.283	4.07 ± 0.12	HMXB	IGR/SAX J18027-2017	98,99
299	IGR J18027-1455	270.692	-14.910	2.05 ± 0.15	AGN	1RXS J180245.2-145432(f)	86,3
300	IGR J18048-1455	271.180	-14.925	1.06 ± 0.15	HMXB		44,60
301	XTE J1807-294	271.770	-29.430	0.95 ± 0.10	LMXB		
302	SGR 1806-20	272.162	-20.404	3.26 ± 0.12	SGR		
303	PSR J1811-1925	272.862	-19.423	0.99 ± 0.13	PSR/PWN	SNR G11.2-0.3	
304	IGR J18135-1751	273.397	-17.858	1.28 ± 0.14	PWN/SNR?	HESS J1813-178	46
305	GX 13+1	273.629	-17.155	11.96 ± 0.14	LMXB		
306	M 1812-12	273.780	-12.094	26.22 ± 0.16	LMXB		
307	GX 17+2	274.006	-14.035	55.95 ± 0.15	LMXB		
308	IGR J18170-2511[c]	274.295	-25.142	0.82 ± 0.11			
309	XTE J1817-330	274.431	-33.020	7.57 ± 0.11	LMXB		
310	SAX J1818.6-1703	274.699	-17.033	1.48 ± 0.15	HMXB		33
311	AX J1820.5-1434	275.112	-14.564	2.19 ± 0.16	HMXB		
312	IGR J18214-1318	275.340	-13.299	1.36 ± 0.15			44
313	4U 1820-303	275.921	-30.362	29.26 ± 0.11	LMXB		
314	IGR J18249-3243	276.206	-32.738	0.92 ± 0.11	AGN	PKS 1821-327?	9
315	4U 1822-000	276.312	0.007	1.59 ± 0.16	LMXB		
316	4U 1822-371	276.447	-37.106	25.61 ± 0.14	LMXB		
317	IGR J18257-0707	276.480	-7.145	1.03 ± 0.15			44
318	LS 5039	276.554	-14.861	0.57 ± 0.16	HMXB		
319	GS 1826-24	277.367	-23.798	73.65 ± 0.13	LMXB		
320	AX J183039-1002	277.660	-10.049	0.84 ± 0.16			
321	IGR J18325-0756	278.112	-7.938	1.89 ± 0.15			100
322	SNR 021.5-00.9	278.394	-10.572	2.88 ± 0.16	SNR		
323	PKS 1830-211	278.421	-21.068	2.34 ± 0.15	AGN		
324	3C382	278.738	32.660	2.77 ± 1.22	AGN		
325	RX J1832-33	278.933	-32.990	9.59 ± 0.13	LMXB		
326	AX J1838.0-0655	279.503	-6.911	2.03 ± 0.15	SNR/PWN	HESS J1837-069	47
327	ESO 103-G035	279.632	-65.422	4.64 ± 0.94	AGN		
328	Ser X-1	279.991	5.041	10.27 ± 0.13	LMXB		
329	IGR J18410-0535	280.262	-5.577	1.11 ± 0.15	HMXB	AX J1841.0-0536	19
330	1E 1841-045	280.329	-4.938	2.48 ± 0.15	PSR/PWN		
331	3C390.3	280.578	79.763	4.30 ± 0.44	AGN		
332	AX J1845.0-0433	281.253	-4.574	1.43 ± 0.14	HMXB		40
333	GS 1843+00	281.404	0.868	4.63 ± 0.13	HMXB		
334	PSR J1846-0258	281.613	-2.983	1.57 ± 0.15	PSR/PWN	AXP?	
335	A 1845-024	282.048	-2.426	0.93 ± 0.13	HMXB		
336	IGR J18483-0311	282.071	-3.172	3.18 ± 0.14			71
337	IGR J18486-0047[c]	282.104	-0.787	1.07 ± 0.13			
338	IGR J18490-0000	282.258	-0.013	1.13 ± 0.13			38
339	4U 1850-087	283.265	-8.702	5.02 ± 0.15	LMXB		
340	IGR J18539+0727	283.500	7.488	0.69 ± 0.12	LMXB?		30,24
341	4U 1849-31	283.761	-31.155	6.40 ± 0.18	CV	V1223 Sgr	
342	XTE J1855-026	283.870	-2.601	10.61 ± 0.13	HMXB		
343	IGR J18559+1535	283.987	15.629	1.59 ± 0.16	AGN	2E 1853.7+1534	32,8
344	IGR J18578-3405	284.469	-34.096	4.01 ± 0.64[R408]	AGN?		
345	XTE J1858+034	284.673	3.437	12.09 ± 0.12	HMXB		
346	HETE J19001-2455	285.039	-24.917	7.03 ± 0.21	LMXB		
347	XTE J1901+014	285.415	1.447	2.59 ± 0.12	HMXB?		69
348	4U 1901+03	285.917	3.207	31.22 ± 0.12	HMXB		
349	SGR 1900+14	286.839	9.322	0.91 ± 0.11	SGR		
350	XTE J1908+094	287.219	9.374	1.45 ± 0.12	LMXB		
351	4U 1907+097	287.406	9.833	14.59 ± 0.12	HMXB		
352	IGR J19108+0917	287.641	9.312	2.70 ± 0.55			
353	X 1908+075	287.701	7.595	13.04 ± 0.12	HMXB		
354	Aql X-1	287.814	0.584	12.30 ± 0.12	LMXB		
355	SS 433	287.957	4.979	8.78 ± 0.11	HMXB		
356	IGR J19140+098	288.526	9.885	8.99 ± 0.12	HMXB	IGR J19140+0951	53,42
357	GRS 1915+105	288.801	10.947	261.49 ± 0.12	LMXB		
358	4U 1916-053	289.686	-5.247	8.04 ± 0.16	LMXB		
359	SWIFT J1922.7-1716	290.615	-17.300	8.38 ± 1.23[R309]			65
360	1H 1934-063	294.422	-6.240	1.24 ± 0.22	AGN		
361	RX J1940.2-1025	295.050	-10.446	2.32 ± 0.28	CV	V1432 Aql	36
362	NGC 6814	295.685	-10.331	3.30 ± 0.29	AGN		
363	XSS J19459+4508	296.887	44.883	1.06 ± 0.31	AGN	IGR J19473+4452 2MASX J19471938+4449425	23,2
364	KS 1947+300	297.397	30.211	13.11 ± 0.30	HMXB		
365	3C403	298.024	2.445	5.18 ± 1.56	AGN		
366	4U 1954+319	298.933	32.094	4.76 ± 0.27	HMXB		
367	Cyg X-1	299.588	35.202	736.49 ± 0.24	HMXB		
368	Cygnus A	299.863	40.736	4.03 ± 0.23	AGN		
369	SWIFT J2000.6+3210	300.101	32.166	1.89 ± 0.26	HMXB	IGR J20006+3210	65,66

Table 1 (cont'd)

Id	Name	RA	Dec	$F_{17-60\ \mathrm{keV}}$	Type	Counterpart	Notes
370	IGR J20187+4041	304.647	40.706	1.32 ± 0.19	AGN	2MASX J20183871+4041003 IGR J2018+4043	26,39
371	IGR J20286+2544	307.140	25.746	2.31 ± 0.41	AGN	MCG +04-48-002	9,7
372	EXO 2030+375	308.062	37.638	33.45 ± 0.19	HMXB		
373	Cyg X-3	308.108	40.959	160.81 ± 0.18	HMXB		
374	4C +74.26	310.576	75.141	2.74 ± 0.85	AGN		
375	MRK 509	311.036	-10.727	3.85 ± 0.58	AGN		
376	IGR J20569-4940	314.215	49.679	1.03 ± 0.22		3A 2056+493	
377	SAX J2103.5+4545	315.901	45.753	10.47 ± 0.18	HMXB		
378	S5 2116+81	318.736	82.045	2.48 ± 0.67	AGN		
379	IGR J21178+5139	319.441	51.650	1.35 ± 0.24	AGN	2MASX J21175311+5139034	9
380	IGR J21237+4218	320.960	42.316	1.03 ± 0.18	CV	V2069 Cyg	
381	IGR J21247+5058	321.161	50.973	5.98 ± 0.24	AGN		86,3
382	IGR J21277+5656	321.930	56.943	1.87 ± 0.31	AGN		32
383	4U 2127+119	322.502	12.172	3.72 ± 0.47	LMXB		
384	CV Cyg	323.449	51.122	3.15 ± 0.26	CV		36
385	IGR J21343+4738	323.625	47.614	1.09 ± 0.21		1RXS J213419.6+473810	
386	SS Cyg	325.711	43.574	2.89 ± 0.22	CV		
387	Cyg X-2	326.170	38.319	25.81 ± 0.23	LMXB		
388	NGC 7172	330.490	-31.864	4.18 ± 0.35	AGN		
389	BL Lac	330.645	42.267	1.31 ± 0.26	AGN		1
390	4U 2206+543	331.992	54.513	6.40 ± 0.25	HMXB		
391	FO Aqr	334.402	-8.301	$3.28 \pm 0.99^{\mathrm{R25}}$	CV		
392	NGC 7314	338.890	-26.021	1.51 ± 0.40	AGN		
393	IGR J22367-1231	339.176	-12.539	1.83 ± 0.39	AGN	MRK 915	
394	IGR J22517+2218[c]	342.939	22.316	$2.45 \pm 0.43^{\mathrm{R316}}$			
395	3C 454.3	343.490	16.143	9.73 ± 0.38	AGN		1
396	MR 2251-178	343.465	-17.616	3.32 ± 0.34	AGN		
397	NGC 7469	345.825	8.879	3.31 ± 0.54	AGN		
398	MRK 926	346.166	-8.689	2.49 ± 0.37	AGN		
399	Cas A	350.846	58.813	3.68 ± 0.11	SNR		
400	IGR J23523+5844[c]	358.079	58.745	0.62 ± 0.10			

[a]Thermal emission dominates.

[b]Spatial confusion, source flux should be taken with the caution.

[c]Newly discovered sources in this survey.

[d]Flux measured in the energy range $15 - 25$ keV over 10 s during the burst (Chelovekov et al. 2006).

[e]May contain flux from ESO 138-G1 (AGN, $\sim 6.5'$from NGC6221)

[R]Source flux was measured on the map averaged over the indicated spacecraft revolution.